ICARUS **135,** 4–24 (1998)
ARTICLE NO. IS985969

Europa: Initial Galileo Geological Observations

Ronald Greeley, Robert Sullivan, James Klemaszewski, and Kim Homan

Department of Geology, Arizona State University, Box 871404, Tempe, Arizona 85287-1404
E-mail: greeley@asu.edu

James W. Head III and Robert T. Pappalardo

Department of Geological Sciences, Brown University, Box 1846, Providence, Rhode Island 02912

Joseph Veverka and Beth E. Clark

312 Space Sciences, Cornell University, Ithaca, New York 14853

Torrence V. Johnson and Kenneth P. Klaasen

Jet Propulsion Laboratory, 4800 Oak Grove Drive, Mail Stop 183-501, Pasadena, California 91109

Michael Belton

National Optical Astronomical Observatory, P.O. Box 26732, Tucson, Arizona 85726-6732

Jeffrey Moore and Erik Asphaug

NASA–Ames Research Center, Mail Stop 245-3, Moffett Field, California 94035-1000

Michael H. Carr

U.S. Geological Survey, Branch of Astrogeological Studies, 345 Middlefield Road, Mail Stop 946, Menlo Park, California 94025

Gerhard Neukum and Tilmann Denk

DLR (German Aerospace Research Establishment), Institute of Planetary Exploration, Rudower Chaussee 5, 12489 Berlin, Germany

Clark R. Chapman

Southwest Research Institute, 1050 Walnut Street, Number 426, Boulder, Colorado 80302

Carl B. Pilcher

NASA Headquarters/Code S, Washington, DC 20546-0001

and

Paul E. Geissler, R. Greenberg, and R. Tufts

Lunar and Planetary Laboratory, Space Sciences Building, University of Arizona, Tucson, Arizona 85271

Received September 5, 1997; revised March 10, 1998

Images of Europa from the Galileo spacecraft show a surface with a complex history involving tectonic deformation, impact cratering, and possible emplacement of ice-rich materials and perhaps liquids on the surface. Differences in impact crater distributions suggest that some areas have been resurfaced more recently than others; Europa could experience current cryovolcanic and tectonic activity. Global-scale patterns of tectonic features suggest deformation resulting from non-synchronous rotation of Europa around Jupiter. Some regions of the lithosphere have been fractured, with icy plates separated and rotated into new positions. The dimensions of these plates suggest

0019-1035/98 $25.00

that the depth to liquid or mobile ice was only a few kilometers at the time of disruption. Some surfaces have also been upwarped, possibly by diapirs, cryomagmatic intrusions, or convective upwelling. In some places, this deformation has led to the development of chaotic terrain in which surface material has collapsed and/or been eroded.

Key Words: **Europa; Europa geology; Galileo; Galilean satellites; jovian satellites.**

INTRODUCTION

Europa is the second of the large Galilean satellites of Jupiter. With a diameter of 3,120 km and a density of about 3.0 g/cm^3, it is comparable in some respects to Earth's Moon, but with important differences. Ground-based infrared spectroscopic observations almost three decades ago (Pilcher *et al.* 1972, Fink *et al.* 1973) showed the surface of Europa to be dominantly water ice. However, near-infrared mapping spectrometer (NIMS) data (McCord *et al.* 1998) reveal the presence of non-ice materials such as sulfates in the mottled terrain. Analysis of the gravity field of Europa derived from Galileo data indicates that the satellite is differentiated into a predominantly H_2O outer shell 100–200 km thick and a deep interior consisting of rocky and metallic material, possibly involving a metallic core (Anderson *et al.* 1997).

The thickness of the outer H_2O shell is consistent with previous estimates of Ojakangas and Stevenson (1989). Parts of this shell could be liquid (Cassen *et al.* 1979). The origin of the H_2O shell is likely associated with heating, dehydration, and differentiation of the interior. In addition to interior sources, Europa is heated by tidal dissipation resulting from the large mass of Jupiter and the eccentricity forced in Europa's orbit by its Laplacian resonance with Ganymede and Io (Cassen *et al.* 1979, Schubert *et al.* 1986).

Previous imaging of Europa by the Voyager spacecraft was at relatively low resolution: Voyager I coverage was 15 km/pixel, while best Voyager II coverage was about 1.8 km/pixel (Smith *et al.* 1979a, 1979b). These images revealed long surface markings, called *lineae* (Davies 1982), and suggesting tectonic processes, a mottled surface, indicating the presence of nonice components, and a paucity of impact craters. Because of the interest stimulated by the Voyager data, coupled with Earth-based telescopic observations and models of the interior, Europa was identified as a high priority for exploration by the Galileo imaging team (Carr *et al.* 1995). First-order questions regarding Europa that can be elucidated by geological studies include: (1) What constraints does geology place on the interior configuration? (2) Is there liquid water presently below the surface and if so, where and in what quantities? (3) How has Europa evolved through time? (4) How do tectonic surface features constrain the thermal history and current heating rate of Europa?

Obtaining definitive answers to these and related questions is unlikely in the near-term. However, the Galileo mission and the Galileo camera (*Solid State Imaging* system, (SSI); Klaasen *et al.* 1984, Belton *et al.* 1992) are providing insight into these issues and enabling the formulation of specific plans for future exploration.

Galileo Imaging Data

The Galileo spacecraft will make 11 orbits around Jupiter in its nominal mission phase. Each orbit is characterized by a close flyby of either Europa, Ganymede, or Callisto and is designated by a letter and a number indicating the satellite and orbit. For example, E-4 indicates that in its fourth orbit, the spacecraft flew closest to Europa. Although highest resolution remote sensing satellite data on each flyby were taken for those satellites with the close flybys, so-called ''nontargeted'' satellite data were also taken on other orbits as appropriate. Galileo images of Europa obtained through orbit E-11 are listed in Table I. In the Galileo Europa Mission (GEM), scheduled to continue operations through 1999, there are opportunities to obtain additional data on at least 8 flybys of Europa. As described in Klaasen *et al.* (1984), the solid state imaging system has 8 filters, centered at 416, 559, 636, 664, 731, 756, 889, and 989 nm. Because of spacecraft limitations, only sparse color data could be obtained in the nominal mission. Preliminary analyses of the color data are given by Clark *et al.* (1997) and Geissler *et al.* (1997).

Figure 1 is a mosaic of Europa assembled from Voyager and Galileo data. Prominent named features are given for reference and are listed in Table II. Proposed names for features seen well in SSI images must be approved by the International Astronomical Union.

PHYSIOGRAPHY

Major surface features and terrain units on Europa were mapped and described by Lucchitta and Soderblom (1982) and Malin and Pieri (1986) using Voyager images. In general, Europa displays little topographic relief, but has a variety of smooth and textured terrains of different spectral properties, along with networks of grooves, ridges and other linear features. Principal terrains include various plains and mottled terrains (Fig. 1). Low-Sun Galileo images reveal isolated mountains and platforms.

Plains

Plains units are subdivided based primarily on albedo. In general the equatorial plains tend to have a low albedo (0.46 for the violet filter; Buratti and Golombek 1988), which could result from ions that have bombarded the surface, removing parts of the ice and leaving a lag deposit of silicates or other non-ice components, including possible organic compounds (Lanzerotti *et al.* 1978, Squyres 1980).

TABLE I
Data Obtained for Europa by the Galileo Solid State Imaging Experiment through the Nominal Mission

Orbit	Number of frames		Center coordinates	Notes
G1	4 full	@ 1.6 km/pxl	(35, 218)	Vgr gap fill, six-color sample of polar terrain, best regional view of either pole during nominal mission
	1 240 lines	@ 1.6 km/pxl	(19, 192)	
	4 full [green, violet, 756, 968]	@ 1.6 km/pxl	(47, 220)	
	2 376 lines [red, 889]	@ 1.6 km/pxl	(47, 221)	
G2	3 color frames (returned 640 × 640 pixel window of each) [green, violet, 968]	@ 6.9 km/pxl	(0, 292)	Low phase photometry in violet, green, 968
C3	4 partial (535, 40, 225, 96 lines)	@ 0.43 km/pxl	(−15, 195)	Wedge-shaped bands, Thera Macula, dark lineae, transition of plains unit to fractured plains unit, terminator view for morphology
	1 40 lines	@ 0.85 km/pxl	(5, 190)	
E4	5 (800,664, 664, 664, and 536 lines)	@ 1.2 km/pxl	(0, 280)	terminator coverage, large macula, dark terrain at high resolution
	1 400 lines	@ 0.63 km/pxl	(6, 323)	
	3 (2 × 400, and 275 lines)	@ 0.13 km/pxl	(−16, 334)	
	4 partial (16–800 lines)	@ 0.03 km/pxl	(6, 323)	
	4 partial (392–800 lines)	@ 0.03 km/pxl	(6, 327)	
E6	2 full	@ 1.7 km/pxl	(−4, 242)	Thera and Thrace Macula, Agenor Linea, plains, triple band intersection, strat relationships, ''iceberg'' chaos, bright plains at high resolution
	2 full	@ 0.28 km/pxl	(−25, 272)	
	6 full	@ 0.18 km/pxl	(12, 271)	
	6 (2 @ 400, 200, 3 @ 125 lines)	@ 0.052 km/pxl	(−26, 280)	
	4 (3 @ 600, 400)	@ 0.052 km/pxl	(12, 274)	
	5 (2 full and 3 @ 680 lines)	@ 0.02 km/pxl	(13, 273)	
G7	1 full	@ 3.2 km/pxl	(0, 149)	Vgr gap fill, low and very low phase photometry, Tyre Macula in green, violet, and 968, near terminator morphology
	6 370 lines [green, violet, 968]	@ 0.4 km/pxl	(36, 183)	
	3 400 lines [green, violet, 968]	@ 0.7 km/pxl	(31, 147)	
	5 (4 full and 1 @ 25 lines)	@ 0.5 km/pxl	(2, 98)	
C9	3-color [green, 756, 889]	@ 12.6 km/pxl	(0, 40)	Global color in green (no OCM), violet, and 968-leading hemisphere, links to C10
C10	3-color [green]	@ 7.3 km/pxl	(0, 283)	Global color in green (IM8), violet and 968-trailing hemisphere, links to C3, E4 & C9
	[violet, 756, 968]	@ 14.7 km/pxl		
E11	4-color [green, violet, 756, 968]	@ 0.29 km/pxl	(2, 225)	samples dark spot, Pwyll ray, wedge-shaped band
	4-color [green, violet, 756, 968]	@ 0.29 km/pxl	(18, 225)	samples triple band, cycloidal band, plains
	10 full	@ 0.23 km/pxl	(−6, 237)	Terminator coverage, Mannann'an crater
	6 full, 1 partial	@ 0.04 km/pxl	(36, 87)	high-resolution morphology of unexplored terrain

Earth-based observations show that polar plains are brighter than equatorial plains (Murray 1975), which could result from poleward migration of ice (Lucchitta and Soderblom 1982).

Galileo multispectral coverage (Fig. 2) at wavelengths between 416 and 989 nm reveals an unexpected subdivision of Europa's mid-latitude bright plains into two units which are distinct in the near infrared (Belton *et al*. 1996, Clark *et al*. 1997). This difference is attributed to ice grain size effects, in which infrared-dark material is composed of larger grains, perhaps indicating differences in surface histories within the plains. However, there might also be some compositional differences between the two units. In comparison with Ganymede and Callisto, the spectral properties of the plains on Europa suggest that there is less dark, nonice material than even the ''iciest'' surfaces seen on Callisto or Ganymede.

Mottled Terrain

Mottled terrain is characterized by low albedo (0.21 in the violet filter; Buratti and Golombek 1988) splotches (Fig. 3). Lucchitta and Soderblom (1982) subdivided mottled terrain into brown and gray units based on colorimetric properties. Brown mottled terrain as observed at Voyager resolution has pitted, hummocky topography and numerous relatively low-albedo patches as large as a few tens of kilometers across set within the mottled terrain. The normalized reflectance spectra of brown mottled terrain are similar to those of brown materials that occur in small spots, referred to as *lenticulae*, described below (Clark *et al*. 1997). The boundary between the plains and the mottled terrain is transitional, with a slight increase in topographic relief in which the mottled terrain is more broadly undulating. Domes, pits, lineae, and ridges are also visible on mottled terrain, as in the plains. Most lineae are discontinuous and appear to be disrupted within mottled terrain. Some are interrupted by flow-like plateaus ranging in size from a few kilometers to several tens of kilometers across. However, in other locations lineae appear to have formed on top of plateaus, perhaps indicating that the formation of mottled terrain was sporadic and contemporaneous with the formation of ridges (Klemaszewski *et al*. 1997). In gen-

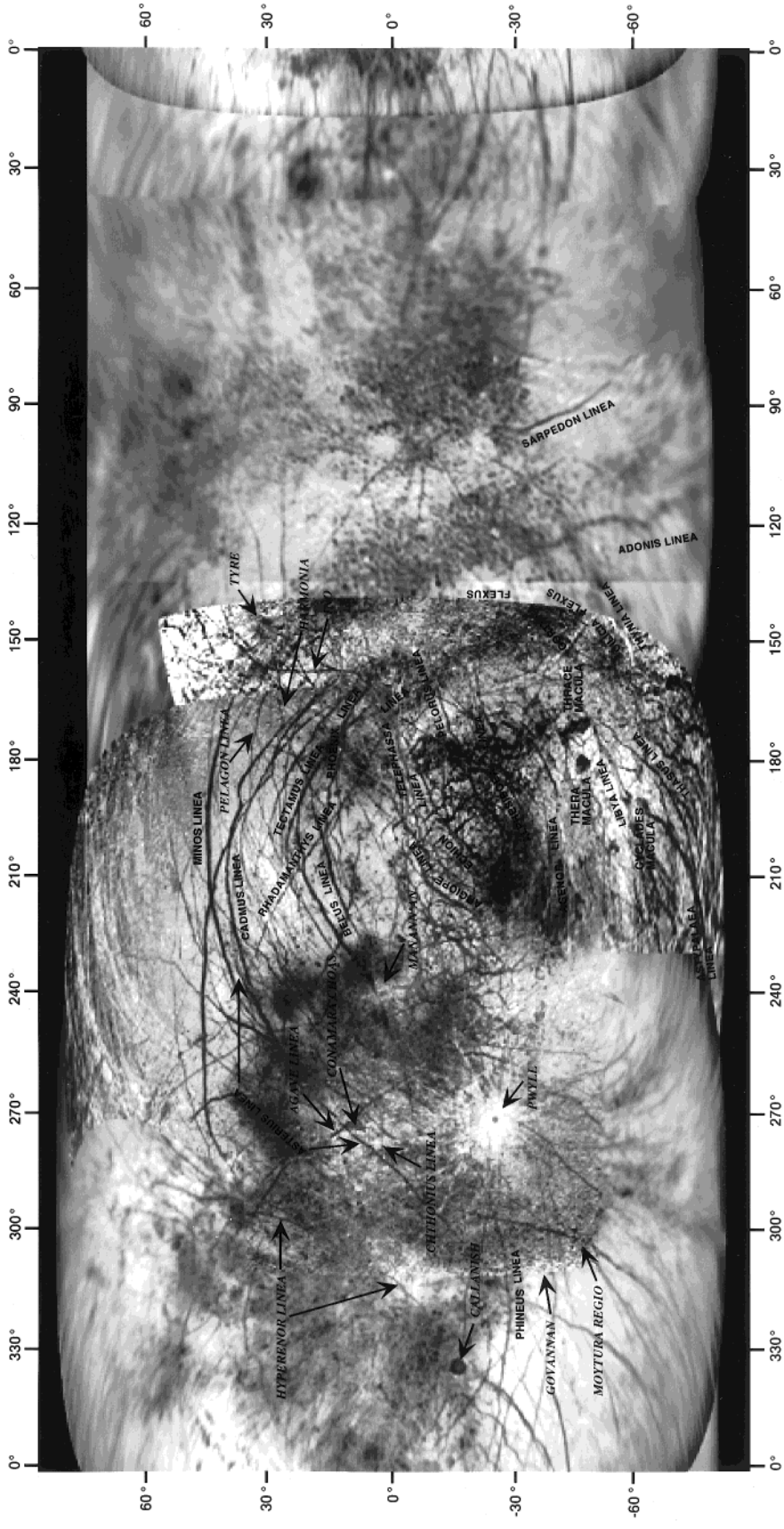

FIG. 1. Mosaic of Voyager and Galileo images for Europa showing some named and newly named (italics) features. In addition to various lineae, the two principal terrains are shown, bright plains and mottled terrain (ASU IPF-1079).

TABLE II
Names for Features Observed on Europa Approved by the International Astronomical Union, 1997

Proposed name	Feature type	Length or diameter (km)	Location		Reference
Agave Linea	linea	1250	7.8 N	267.9 W	Daughter of Harmonia and Cadmus
Callanish	ring	100	16.3 S	333.5 W	Major stone circle in the Outer Hebrides of Scotland
Chthonius Linea	linea	1850	3.8 N	288.2 W	Survivor of the men Cadmus sowed with the dragon's teeth, founder of Thebes
Conamara Chaos	chaotic terrain	99 × 110	9.5 N	273.3 W	Rugged, isolated part of western Ireland named for Conmac, son of Queen Maev
Govannan	crater	10	37.5 S	302.6 W	One of the Children of Don, a smith and brewer
Harmonia Linea	linea	925	28.5 N	168.3 W	Wife of Cadmus
Hyperenor Linea	linea	2200	15.1 N	303.1 W	Survivor of the men Cadmus sowed with the dragon's teeth, founder of Thebes
Ino Linea	linea	1400	6.2 N	161.2 W	Daughter of Harmonia and Cadmus
Manann'an	crater	30	2.0 N	240.0 W	Irish sea and fertility god
Moytura Regio	mottled terrain	235 × 65	47.9 S	297.1 W	Scene of two famous battles between the Celtic DeDanaan and the pre-Celtic tribes the Fir Bolg and the Fomorians
Pelagon Linea	linea	800	33.7 N	170.6 W	King who sold Cadmus a cow marked with a white full moon on each flank
Pwyll	crater	50	25.5 S	271.0 W	Head of Hades and Prince of Dyfed
Tyre	ring	155	30.0 N	145.1 W	Seashore where Zeus carried Europa away

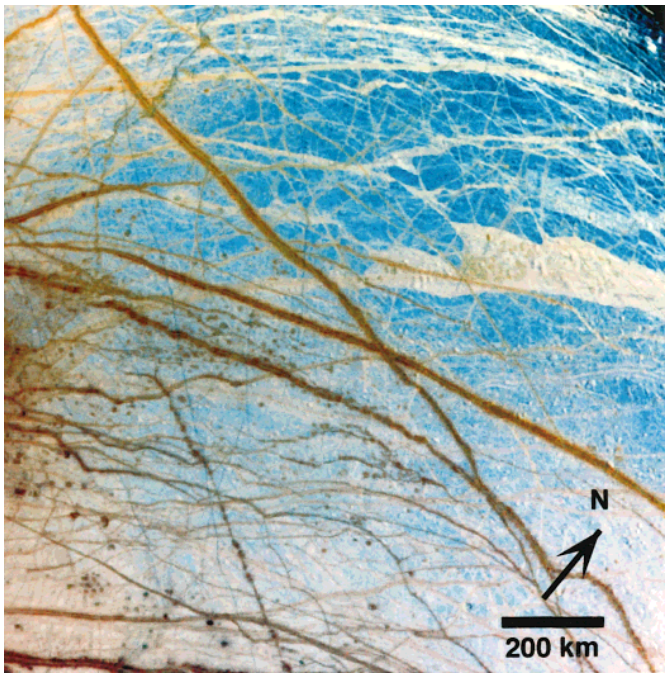

FIG. 2. False-color composite image of part of Europa centered at 45°N, 221°W covering an area 1260 km wide; north is oriented toward the upper right and image resolution is 1.6 km per pixel. This image was derived from frames taken through filters with wavelengths centered at 989, 757, and 559 nm. Triple bands, other lineae, and mottled terrain appear in brown and reddish hues while icy plains (blue and tan hues) subdivide into units with different albedos at infrared wavelengths (from Belton *et al.* 1996; JPL P–47906).

eral, brown mottled terrain appears younger than—and forms at the expense of—bright plains.

In high-resolution Galileo images (Fig. 4), some brown mottled terrain is seen to consist of regions where the surface has been disrupted and broken into plates as small as a kilometer across that have been moved laterally into new positions. The ''mottling'' results from the high-albedo surfaces of the plates set within the lower albedo of the intervening disrupted surface. However, mottling is also present where this style of disruption is absent. The low albedo could result from the exposure of nonice materials or from larger ice grains, or a combination of these two possibilities. Analysis of NIMS data of mottled terrain indicates a lack of water ice and the presence of hydrated minerals on the surface (Fanale *et al.* 1998).

Gray mottled terrain displays albedo characteristics (0.36 in the violet filter; Buratti and Golombek 1988) similar to both brown mottled terrain and the plains units. Gray units are of more limited areal extent in the regions seen on Voyager and have been observed only in moderate resolution by Galileo. Like brown mottled terrain, gray mottled terrain comprises relatively low-albedo patches ranging in size from a few kilometers to several tens of kilometers across, which are transected by numerous lineae. The topography of gray mottled terrain seen in Galileo images is transitional between brown mottled terrain and plains units. It is less hummocky and has more intact lineae than brown mottled terrain, but it is more disrupted than plains units (Klemaszewski *et al.* 1997). The normalized reflectance spectra of gray mottled terrain closely resemble

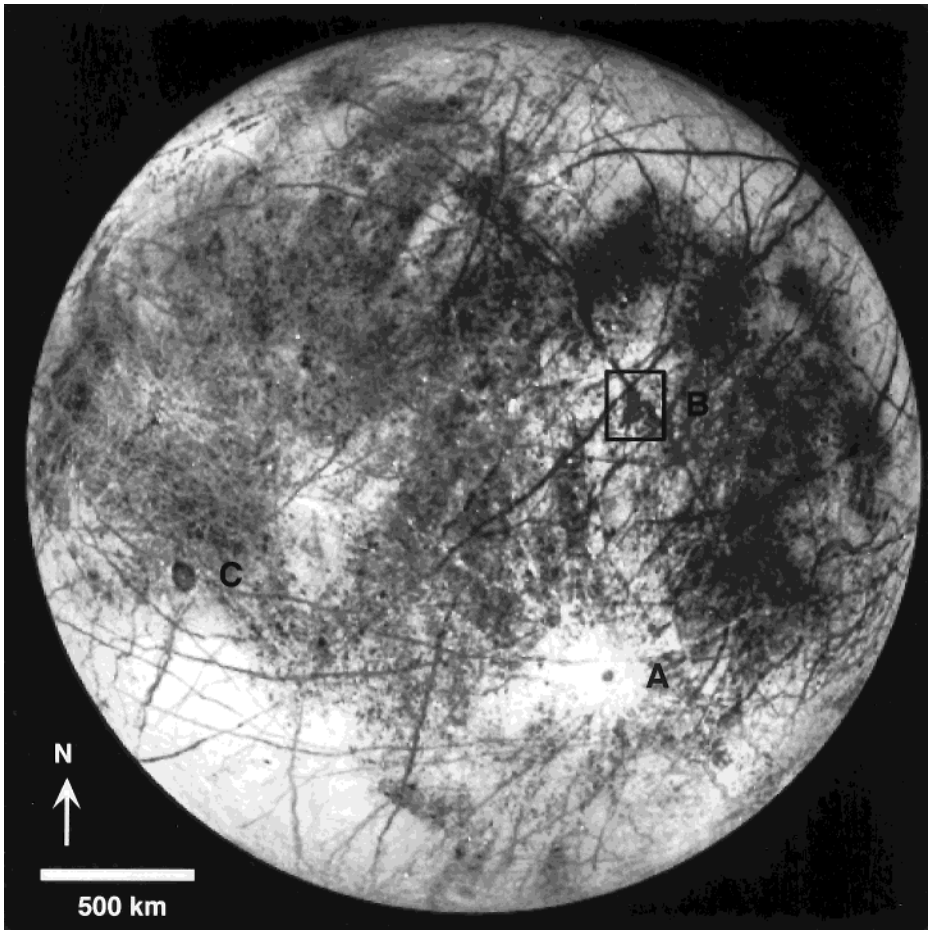

FIG. 3. Galileo image of the trailing hemisphere of Europa centered at the equator and showing a young impact crater (A), named Pwyll, identified by its bright icy ejecta. Numerous lineae are visible, including those forming an "X" pattern ((B), north of Pwyll) imaged in high resolution (Fig. 5). A suspected impact structure, named Callanish is visible as the dark spot on the western (left) side of the disk (C) (Galileo frame S0360063913).

those of the dark and bright plains and bright craters (Clark *et al.* 1997).

Mountains and Plateaus

Although Europa is relatively smooth, topographic features with relief generally less than a few hundred meters are seen in high-resolution Galileo images taken under low-solar illumination. These include raised platform-like areas as large as 35 km across and small mountains. Other isolated massifs include a conical knob 12 km in diameter near 34.5N, 169.5W that is 2 ± 0.5 km high.

GEOLOGIC FEATURES

Craters

One prominent impact crater is Cilix. Identified on Voyager images, Cilix is some 16 km across surrounded by lower albedo material. Cilix is the reference feature on which Europa's geographic longitudes are based (Davies 1982).

The general paucity of impact craters observed in the Voyager data suggested a youthful surface and the possibility of recent, or even active resurfacing (Lucchitta and Soderblom 1982). The increased resolution and coverage afforded by Galileo reveal more impact craters, especially in some areas. These include a 30-km diameter crater *Manann'an*, centered at 2°N, 240°W, *Pwyll*, a 26 km diameter crater centered at 26°S, 271°W previously suggested to be an impact crater based on Voyager data (McEwen 1986a), small (<10–15 km in diameter) craterforms, some of which have raised rims and ejecta patterns, and dark spots, formerly called *maculae*, some of which are of probable impact origin.

From relationships in the exposed rim of Manann'an, the impact appears to have penetrated through dark mottled terrain into bright, presumably ice-rich materials, ejecting

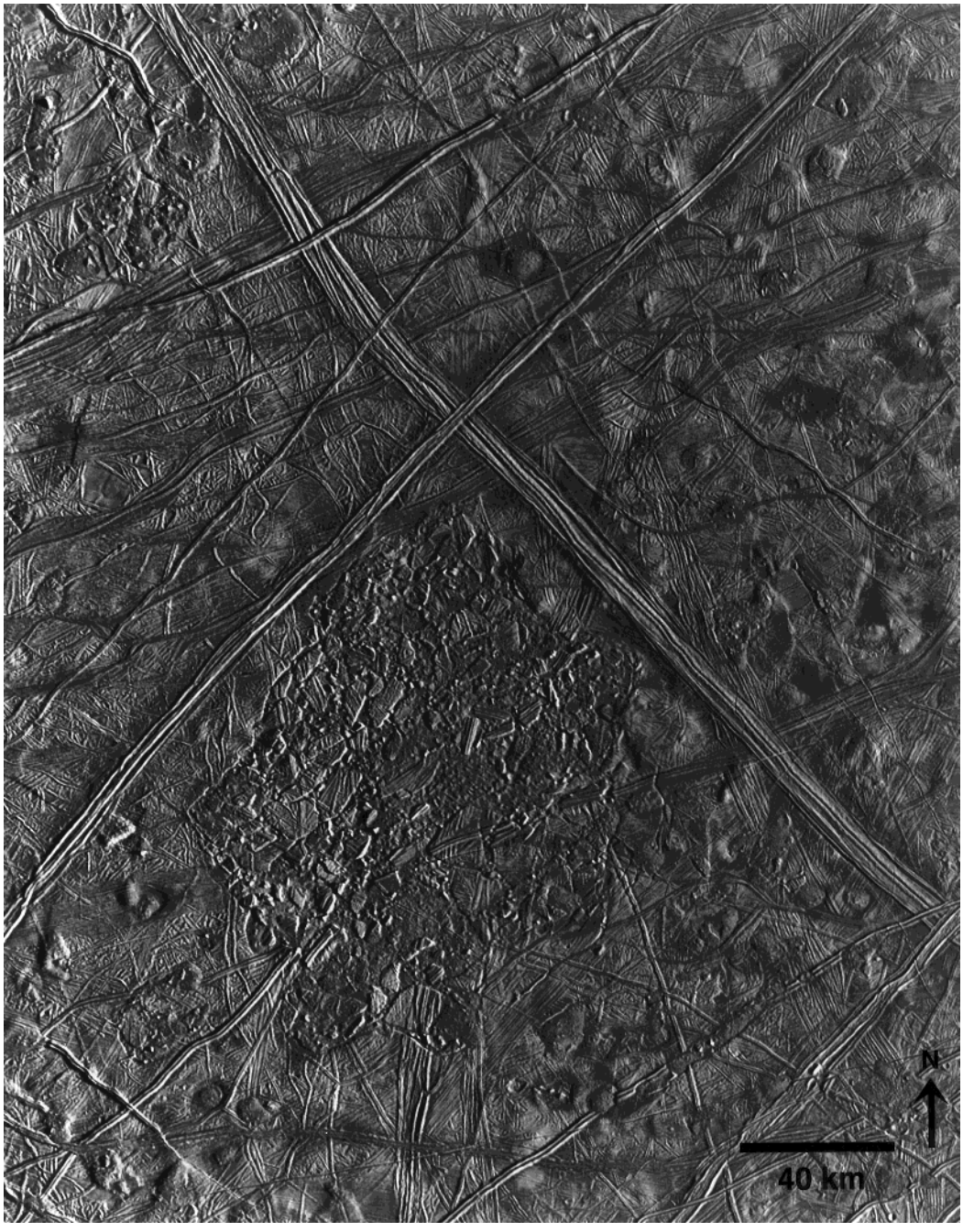

FIG. 4. Mosaic of moderate resolution (180 m/pixel) Galileo images showing the "X" intersection of the triple bands Asterius and Agave lineae seen in Figure 3. In this near-terminator view (illumination from the east, or right), the low albedo flanking stripes of triple bands are poorly seen, while topographic features, such as the complex ridges and grooves of the medial part of the triple bands, are enhanced. Also visible in this image is the zone of mottled terrain (Conamara Chaos) immediately south of the "X." Area shown is about 235 by 290 km (ASU IPF-1112).

discontinuous rays over the surrounding terrain for distances exceeding several hundred kilometers. In contrast, Pwyll crater (Fig. 5) appears to have excavated relatively red low-albedo material, which forms a dark zone on the floor of the crater and blankets the surrounding terrain nearly 1 crater radius from the rim. Pwyll has an irregularly shaped central peak complex about 8 km across. Its floor appears to be nearly the same elevation as the surrounding terrain, suggesting substantial rebound following the impact, or flooding of the crater floor by melt resulting from the impact. The bright ejecta rays from Pwyll can be traced more than 1000 km across Europa and are superposed on

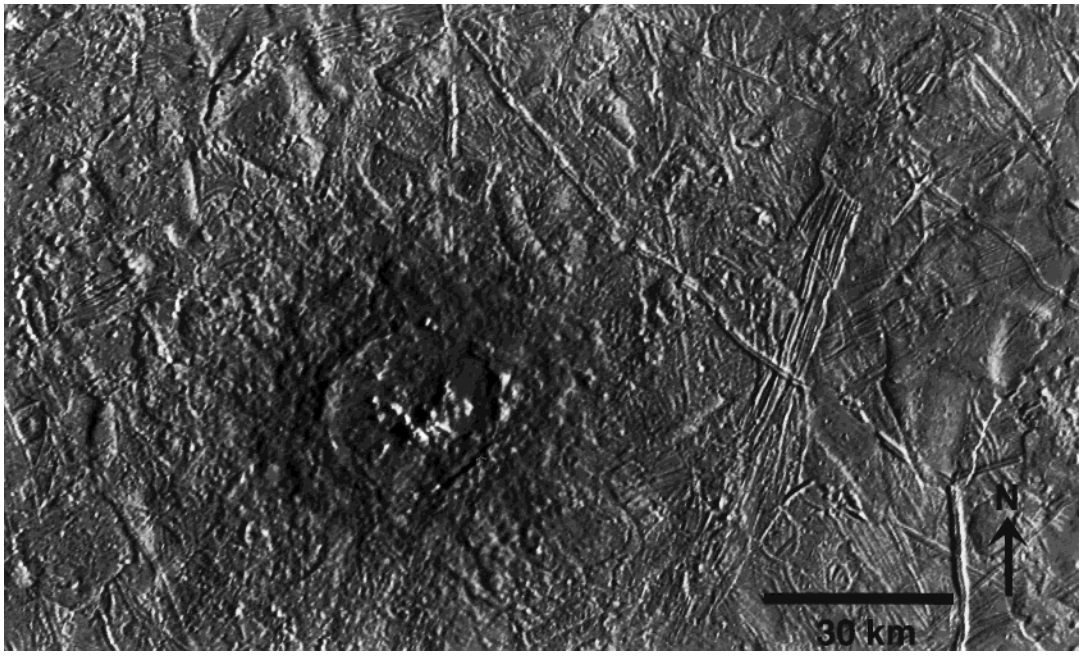

FIG. 5. Mosaic of two Galileo images showing Pwyll, the prominent impact crater seen in Figure 3. The dark area visible in the global view coincides with the dark ejecta deposits, but does not signify the crater rim diameter. The crater rim is about 26 km across. In addition to the central peak cluster, the crater floor appears to stand as high or higher than the surrounding terrain, suggesting flooding or rebound of the crater bowl following the impact. Area shown is about 160 by 100 km; resolution is 240 m/pixel and illumination is from the east (right) (JPL P-48506).

many of the ridges and other geologically young terrain features (Fig. 3).

The topography of the rims for Manann'an and Pwyll craters and the central peak of Pwyll suggest that the outer H_2O shell of Europa was sufficiently rigid at the time of the impact for these features to form and be preserved. From depth to diameter relations for the transient cavity (Melosh 1989), the rigid ice shell in the area impacted must have been at least 10–15 km thick in order for a central peak to have formed and been preserved.

Small (<5–6 km in diameter) impact craters with patterns of radial ejecta are seen in many areas on Europa. Some of these craters have ejecta deposits that are of lower albedo than that of the plains on which they were emplaced (Fig. 6). With such small diameters, this suggests that the depth to a substrate zone of darker material is shallow, perhaps less than a few hundred meters deep, at least locally. Alternatively, the dark material in and around some craters may be melt produced by impact into a porous surface, in which rapid closure of pores in a loose regolith leads to greatly enhanced shock heating (e.g., Zel'dovich and Raizer 1967). Craters lacking dark ejecta may have formed in a comparatively nonporous target. In these cases, the impact might have penetrated an outer ice-rich layer into a subsurface zone containing a higher abundance of nonice components.

Numerous shallow depressions are observed in images taken of the terminator zone. Although some of these depressions have irregular shapes suggestive of endogenic origin (Chapman *et al*. 1997), others are circular and some have slightly raised rims, characteristic of impact craters.

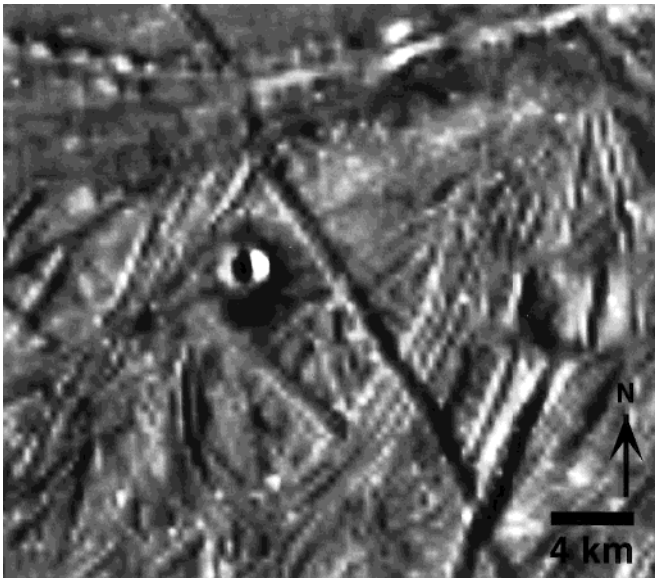

FIG. 6. Image of a 2 km in diameter impact crater centered at 16°S, 198°W, showing low albedo ejecta and raised rim (Galileo frame S0368639400).

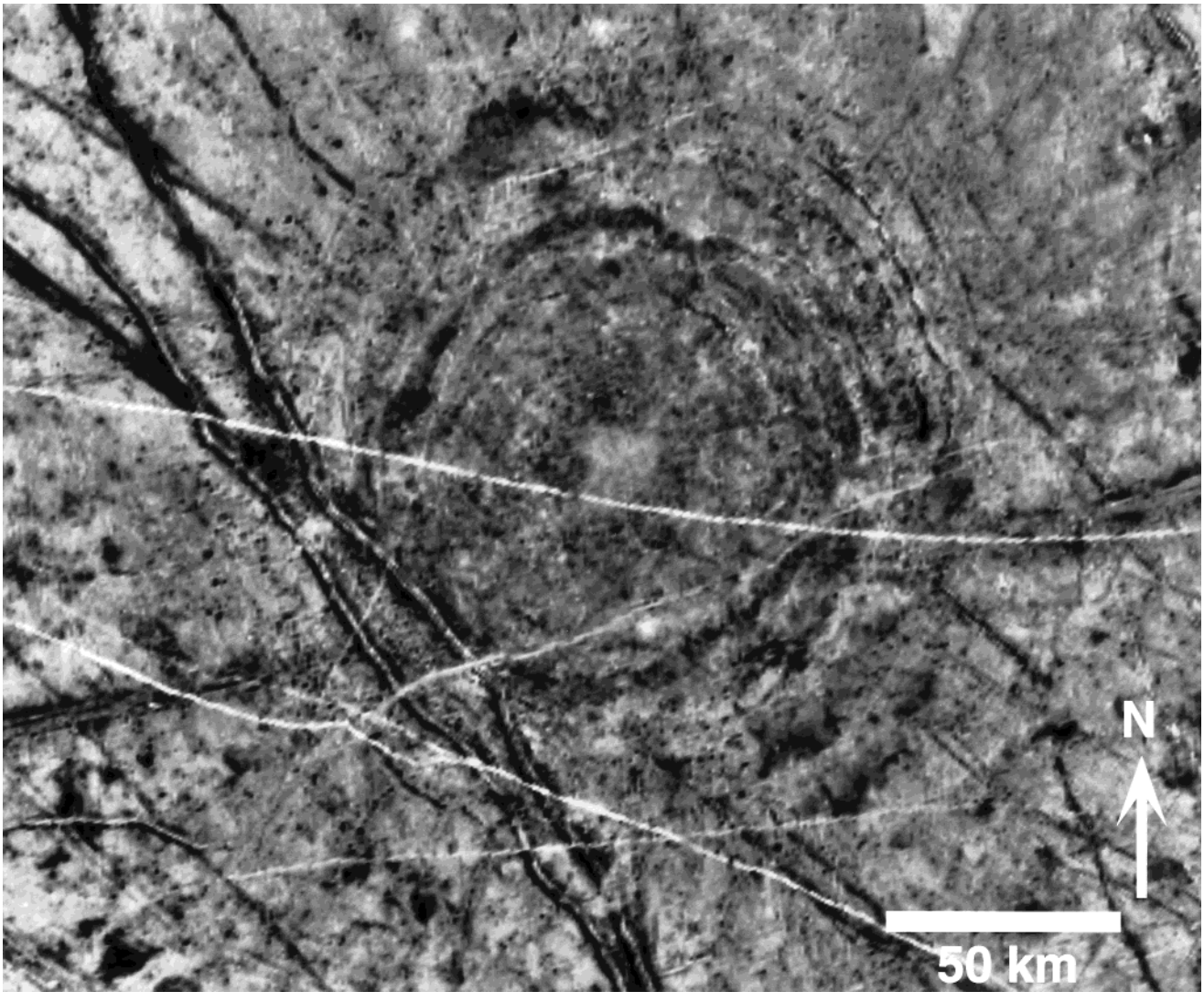

FIG. 7. Galileo image of Tyre, showing concentric low albedo patterns, triple bands that cross-cut the concentric structures, and very narrow bright bands. Also visible are irregular shaped low albedo spots (lenticulae), in the lower left corner. Note that the low albedo components of the triple bands are not symmetric about the central bright band. Area shown is 250 by 200 km; north is to the top (Galileo frame SO389772507).

If these features are impact craters, then some areas on Europa are older than inferred from Voyager data. However, other areas observed under comparable illumination and resolution are very smooth and lack depressions of any type, suggesting local, geologically recent resurfacing (Belton *et al.* 1996).

Various low-albedo features, referred to as *maculae*, were identified on Voyager images. Some of these features exceed one hundred kilometers in diameter. One, named Tyre, was imaged on Galileo's 7th orbit at 670 m/pixel resolution (Fig. 7). It is an oval feature 160 by 120 km across previously speculated to be of impact origin (Lucchitta and Soderblom 1982, Malin and Pieri 1986). It includes concentric low-albedo discontinuous bands, some of which appear to be ridges. In Galileo images, the center of Tyre is seen to contain a smooth high-albedo zone some 18 km across. The western margin of the structure is crosscut by two prominent lineae. However, outer parts of Tyre appear to be superposed on fainter, older linear features. The youngest features visible in this area are narrow (~1 km) high-albedo lineae which crosscut Tyre and all other features in the area. Thus, the formation of Tyre occurred when the crust of Europa was being tectonically disrupted by the formation of ridges and lineae.

A large circular feature (Figs. 3 and 8) resembling Tyre was imaged by Galileo at 16°S, 334°W (Moore *et al.* 1997) and named *Callanish*. Callanish can be divided into an inner zone 50 km across characterized by a rugged surface

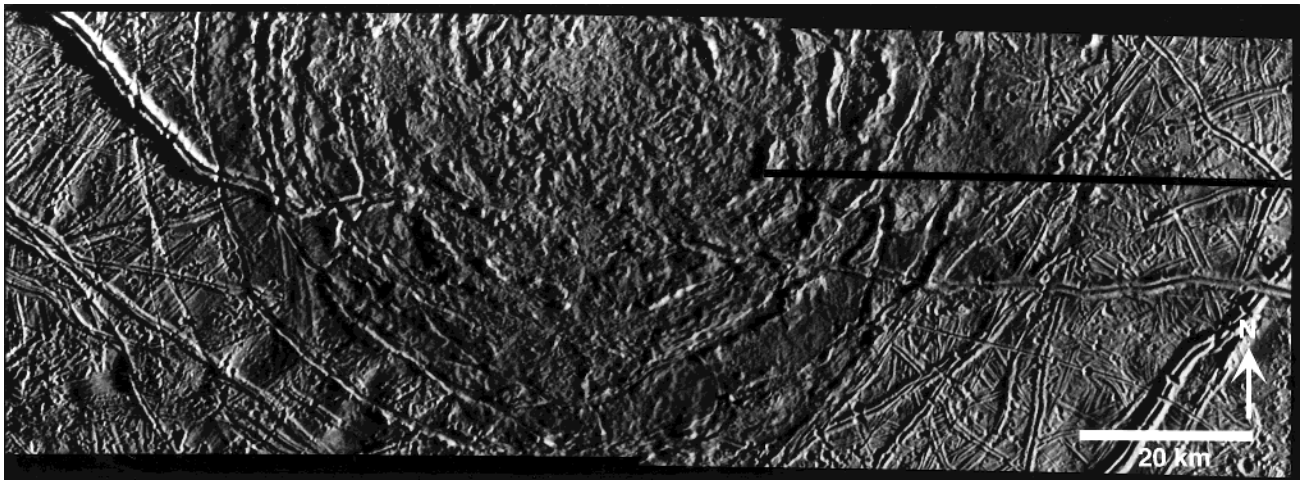

FIG. 8. Moderate resolution (130 m/pixel) image showing part of the ring feature, Callanish, shown in Figure 3; it is centered at about 16°S, 334°W and is about 100 km across; illumination is from the east, or right side of picture. The concentric fractures, disrupted central terrain, and presence of numerous small craters outward from the fractures support an impact origin for this feature and might indicate a relatively thin lithosphere overlying liquid or ductile material that was unable to preserve a craterform depression (JPL P-48228).

and an outer zone containing small (~2–3 km across) hills disrupted by tectonic features dominated by two concentric troughs or possible graben. The style and dimensions of the troughs suggest that the depth to a mechanical discontinuity is ~500 m if the bounding fractures are faults dipping ~60°. Numerous small depressions, some with raised rims, are found in the area surrounding Callanish. Some form chains of pits oriented radially to the feature and could be secondary craters.

In some respects, Callanish resembles coronae on Venus, which are thought to result from mantle upwelling and crustal deformation (Stofan *et al.* 1992). However, the presence of craters similar to secondaries and the style of deformation of Callanish suggest an impact origin similar to palimpsests seen on Ganymede (Smith *et al.* 1979a). If of impact origin, the low relief of the feature on Europa could have resulted from slow, viscous relaxation of the rim, as proposed for palimpsests and other topographic features on icy satellites (Shoemaker *et al.* 1982, Passey and Shoemaker 1982, Jones *et al.* 1997, and others), or rapid deformation of the craterform immediately following impact (Croft 1983), as demonstrated in laboratory-scale impacts into thin ice over a liquid substrate (Greeley *et al.* 1982). From the relationships seen in Callanish, we conclude that it and similar features on Europa are probably of impact origin.

A faint multiringed feature is seen on the antijovian hemisphere centered at 20°S, 203°W and could reflect an ancient impact (Carr *et al.* 1997). Although the multiringed nature of the feature is difficult to discern in Mercator projections, it is more apparent in stereographic projections (Fig. 9). The rings are defined by low-albedo lineae and by the boundaries between mottled terrain and bright plains. The most prominent ring segments are (1) to the north, part of Belus Linea at a radius of 1120 km from the center of the structure and Minos Linea at 1750 km radius, (2) to the southeast, Adonis Linea at 1860 km radius and Sarpedon Linea at 2650 km radius, and (3) to the east, the feature is defined by the boundaries between plains and mottled terrain at 1300, 1800, and 2200 km radii. Numerous other dark lineae form arcs around the same center. The central region of the feature is characterized by a complicated pattern of dark wedges and arcuate dark bands, interpreted as a ''pull-apart'' zone, described below.

Arcs delineating the multiring feature constitute only a few of the arcuate patterns on the antijovian hemisphere. Many others cross the feature and appear unrelated. The origin of the faint, multiringed feature is unclear. It may be a fortuitous combination of arcs that gives the impression of a multiringed structure. On the other hand, the silicate subcrust beneath the H_2O shell could retain the early history of heavy bombardment, and this feature could reflect an impact scar.

Flows and Flowlike Features

Implicit in discussions of ''resurfacing'' on Europa is the concept that icy materials are extruded from the interior onto the surface as liquids or in the solid state. Liquids could be water or slurries of water and ice (i.e., ''slush'') with other nonwater components. The process involving the release of these materials in cold environments either explosively (e.g., geysers) or as surface flows is termed *cryovolcanism*. As reviewed by Kargel (1995), most cryo-

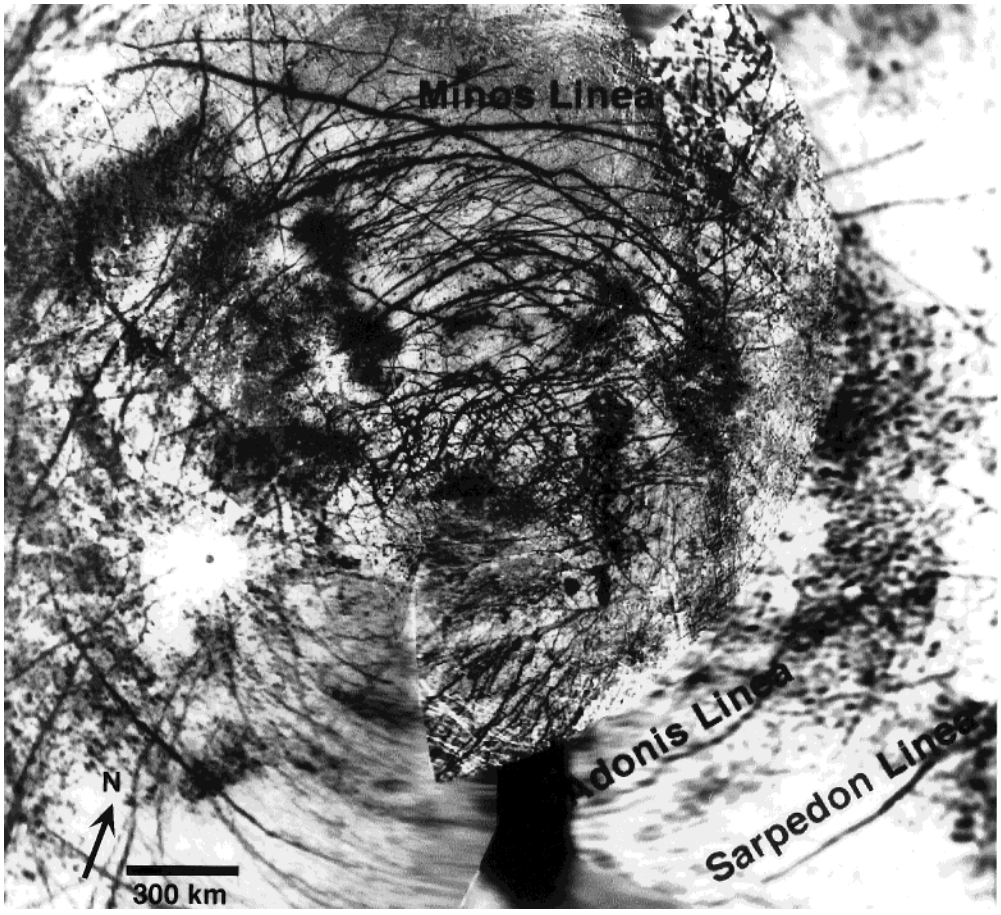

FIG. 9. Mosaic of Voyager and Galileo images in a stereographic projection centered at 20°S, 203°W, showing concentric pattern of lineae and boundaries between mottled terrain and plains.

volcanic events are unlikely to involve pure water because it is difficult for water to reach the surface through the lower density ice crust. In addition, pure water is highly reactive with many silicate minerals and electrically polar substances that form nonwater ices. Models involving water combined with ammonia (Kargel 1991, Kargel *et al.* 1991) or charged with CO_2 or other volatiles (Crawford and Stevenson 1988) have shown that cryovolcanism can be an effective process of surface modification. In addition, overpressurization by tectonic processes of subsurface zones could enable liquid or solid-state extrusions onto the surface (Wilson *et al.* 1997).

Figure 10 shows the region centered at 5.2°N, 319.5°W imaged at moderate resolution (630 m/pixel). This region is transitional between plains and mottled terrain. In some areas, lobate features intersect ridges, apparently having either flowed through gaps, intruded into the ridges from below, or eroded through the ridges, perhaps by thermal processes. The possible flow lobes are as high as 250 m, suggesting that they were rather viscous during emplacement. None appear to have flowed more than 25 km. Unfortunately, none of the specific flow-like features were imaged in higher resolution. Figure 11 shows part of this terrain in high resolution and illustrates modification of the surface. Some areas show gentle to moderately upwarped surfaces with medial fractures (Fig. 11a). In other areas, there is more relief and the surface has a muffin-like surface (Fig. 11b) superposed on existing topography. Still other terrains show a chaotic topography with highly disrupted surfaces (Fig. 11c).

The terrains shown in Fig. 11 are suggested to represent endogenic processes, perhaps in different stages of surface modification. Figure 12 shows cross sections based on the images in Fig. 11. The vertical arrows represent uplift which could result from magmatic intrusion, diapirs (low-density masses), or thermally driven convection. In case 3 (Fig. 11b), the mass represents either extrusion or mobilization of the icy crust into a flow. The short, stubby morphology suggests a relatively viscous mass. In cases 4 and 5 (Fig. 11c), material appears to have been removed, either by collapse, erosion of volatile components, or by surface flow (small channel-like features are present). Figure 13 shows

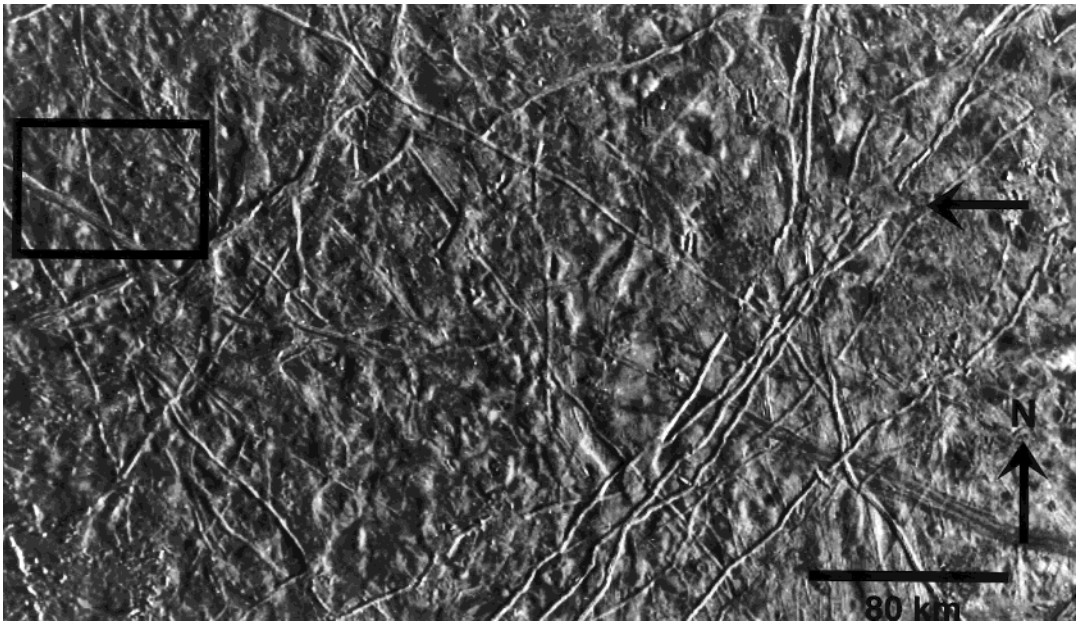

FIG. 10. Moderate resolution (634 m/pixel) image showing hummocky terrain centered at 6°N, 322°W; note that some ridges have superposed flowlike masses (arrow). Outline shows area seen in higher resolution (Fig. 11). Illumination is from the east (right); area shown is about 440 by 280 km (Galileo frame S0374667300).

another area on Europa where the surface has been modified by endogenic processes similar to those outlined in Figs. 11 and 12.

Low to moderate resolution (>2 to ~0.5 km) images of the europan surface show irregular shaped low-albedo spots as large as ~20 km across. Provisionally termed *lenticula*, these spots occur as isolated features or in clusters. Higher resolution images show that some lenticula consist of domes or low, rounded hills (Fig. 4). In some cases, these appear to be relatively unaltered parts of the crust that have been slightly upwarped from below. In other cases, the domes appear to consist of material derived from the interior that broke through to the surface as a viscous mass (Fig. 13). Pappalardo *et al*. (1997) suggest that the pits and domes of some lenticula represent solid-state convection in the icy shell, as predicted if the shell is thick (>7 km) and underlain by a warm layer, such as liquid water.

Low-viscosity surface flows are suggested by Fig. 11d, which shows ridged and grooved terrain that appears to have been locally flooded to produce a nearly flat, smooth surface. This is a very high resolution image (25 m/pixel), and the flooded material shows no raised margin, even in this near-terminator view in which visibility of topographic relief is enhanced. This suggests that the material was very fluid at the time of emplacement, and water or a water-rich solution is a reasonable candidate composition. An alternative mechanism to produce the flat surface shown in Fig. 11d involves heating from below with melting or mobilization of surface materials without extrusion. In either case, the high frequency of impact craters superposed on the flooded area indicates that the surface is relatively old, although many of the craters could be secondaries. In other areas, however, flow-like features lack impact craters and were apparently formed in geologically recent times.

Images of the region centered at 10°N, 271°W (named Conamara chaos; Figs. 3 and 4) show parts of the ridge and grooved terrain that have been severely disrupted, with blocks of icy crust as small as 1 km being shifted into new positions (Fig. 14). The heights of these blocks range from <25 to 200 m above the lower, rough terrain. We suggest that the blocks must have been underlain by mobile materials, potentially water-rich at the time of disruption, and that their displacement occurred as a result of convection within the substrate (Belton *et al*. 1997, Pappalardo *et al*. 1997).

Tectonic Features

Voyager and Galileo images show the surface of Europa to be crisscrossed by a variety of linear, curvilinear, and wedge-shaped structures suggesting tectonic activity (Lucchitta *et al*. 1981, Sullivan *et al*. 1997, and others). Lineae (Davies 1982), constitute the principal structural features on Europa (Lucchitta and Soderblom 1982). They extend hundreds or even thousands of kilometers and are most prominent in plains areas (Fig. 1). Many lineae identified

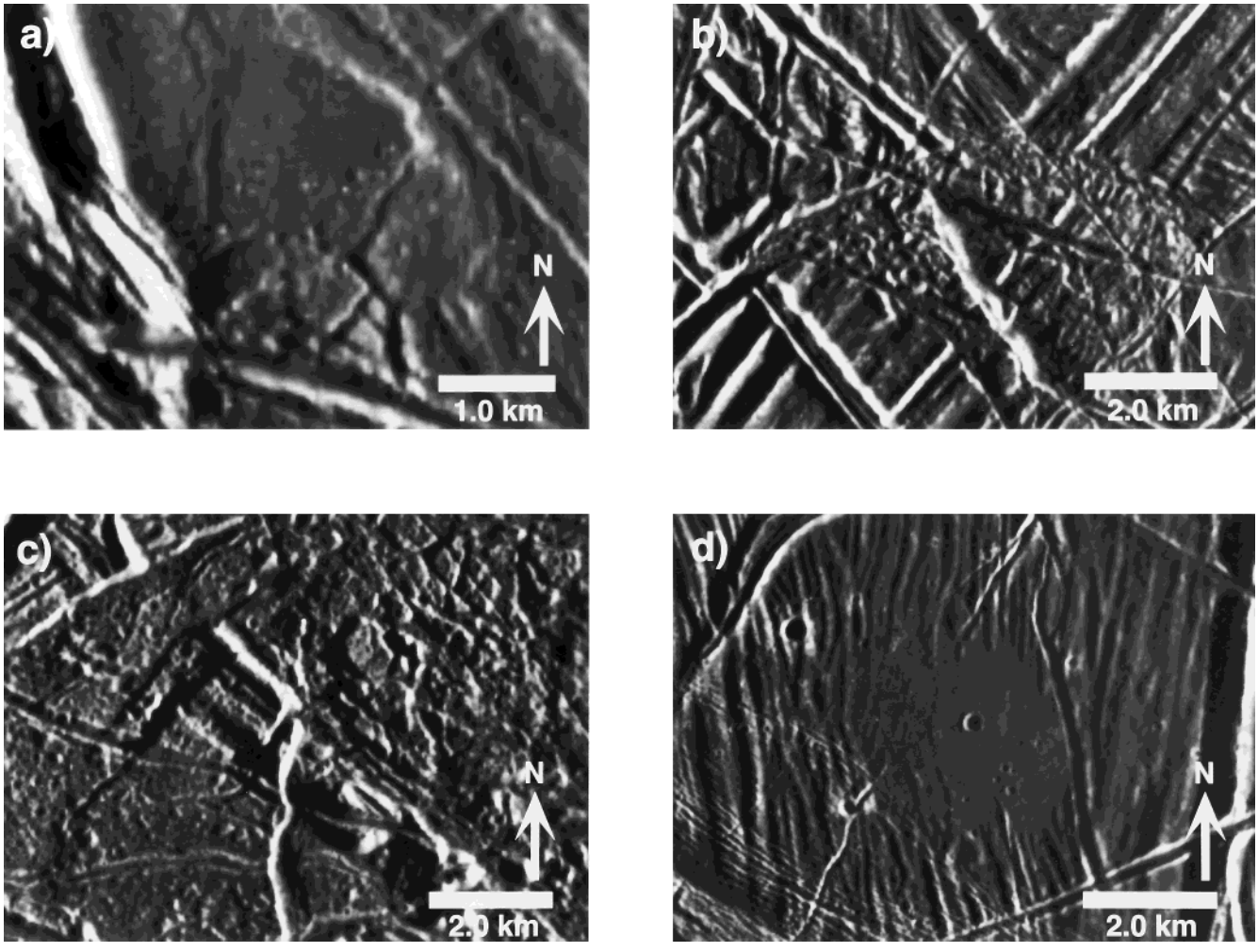

FIG. 11. Detail (~25 m/pixel) of area shown in Figure 10; a) gentle dome with irregular medial fracture; superposed by a second dome that is more highly fractured; area shown is 4.5 by 3 km (ASU IPF-1048). b) domical mass superposed on ridges and grooves; area shown is 8.7 by 6.3 km (ASU IPF-1048). c) chaotic terrain showing highly disrupted surface and remnant knobs; area covers 8.7 by 6.3 km (ASU IPF-1048). d) small smooth zone superposed on ridged terrain; surface is peppered with small craters of presumed impact origin; area shown is 8.7 by 6.3 km (ASU IPF-1048).

on Voyager images as albedo features are seen in Galileo images to be ridges or ridge-complexes with relief of tens of meters. Most lineae are thought to originate as tectonic features.

Triple bands (TB) are lineae characterized by low albedo stripes typically 10–20 km wide with a medial high-albedo band (Figs. 2, 4, and 7). They occur in a wide variety of morphologies, including TB which merge into simple bright bands or single dark bands, and TB in which the low-albedo component breaks up into discontinuous flanking patches which may be either symmetric or asymmetric about the central bright zone. Most bright bands of TB imaged at high resolution under low solar illumination consist of complex ridges which generally have a prominent medial groove which is probably a fracture (Fig. 15). Crosscutting relations indicate that the low-albedo components of TB tend to brighten with time (Fig. 16), approaching the albedo of the background plains in which they occur (Belton *et al.* 1996, Clark *et al.* 1997).

The darker, brownish parts of the triple bands and the mottled terrain are areas with the highest amount of nonice components on Europa. Their spectral properties at long SSI wavelengths are similar to those of dark terrain on Ganymede and Callisto, while at short wavelengths, they are among the reddist in the visible, even in comparison with Ganymede and Callisto. This could be attributed to larger amounts of sulfur in the dark material on Europa compared to Ganymede and Callisto. This is consistent with the suggestion by Spencer *et al.* (1995) that sulfur

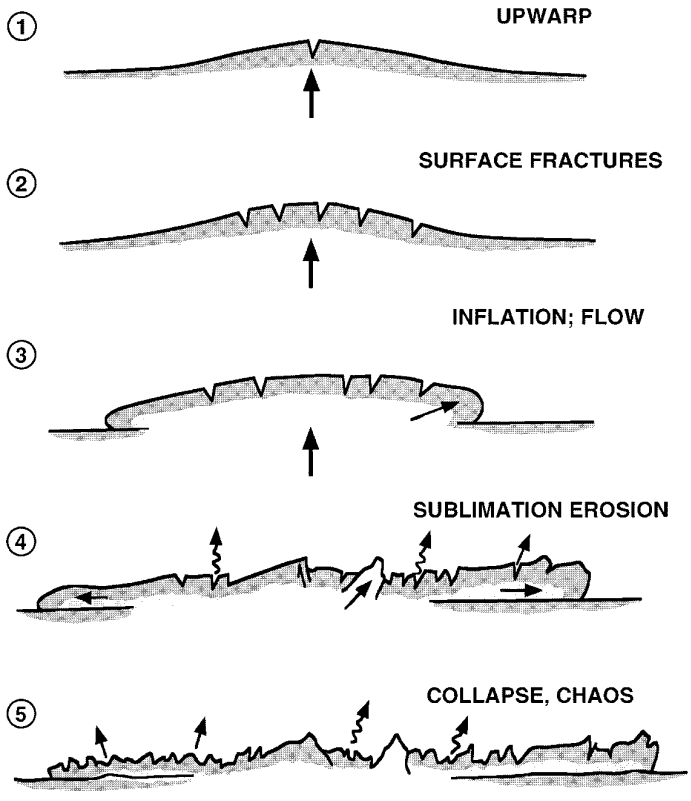

FIG. 12. Diagrams showing interpretation of processes involved in the formation of the features in Figure 11. Arrow represents upwarping from magmatic intrusion, diapiric uplift, or convection.

might be partly responsible for the short-wavelength properties seen in Earth-based spectra of Europa's surface.

Various models were proposed from Voyager images to explain the origin and evolution of TB, including tectonic models involving block faulting and flooding by water or slush (Golombek and Bruckenthal 1983), intrusion of the icy crust by hydrated silicate materials with subsequent dehydration (Finnerty *et al.* 1981), and extrusion of icy material onto the surface. Galileo images show that the outer margins of TB are diffuse and, in some cases, discontinuous (Fig. 7). Consequently, formation models for the dark stripes involving primarily tectonic processes and intrusions, both of which form sharp outer boundaries, are less plausible.

Explosive venting, or ''geysering'' of material from fractures could produce the diffuse outer margins of TB by pyroclastic deposition concentrated close to the vent and thinning to outer feather edges. In this model (Fig. 17), initial eruptions involve gases (proposed by Crawford and Stevenson 1988), and perhaps liquids charged with rocky material derived from the icy crust. As this material reaches the surface, the volatiles condense and the rocky debris showers onto the surrounding terrain. With continued eruption, the conduit is cleared of contaminants, and cleaner slush is exposed to the surface where it freezes, forming the bright medial band.

However, the ''geyser'' model might not explain the complex, interbraided parts of the medial ridge seen in high resolution, nor the great length (hundreds of kilometers) of many triple bands. Pappalardo and Coon (1996) proposed that some ridges and TB form by repeated tensional and compressional tidal stresses which open and close the icy lithospheric plates, resulting in repeated deformation of ice to form complex ridges. The geyser model might be invoked to explain the low-albedo component; as the plates separate during tension, volatile-charged slush containing nonice components could be released to the surface to produce ''dirty'' geysers.

One particularly prominent zone of complex tectonic deformation, informally referred to as a ''pull apart zone,'' is centered approximately in the antijovian region (Fig. 18). It is interpreted as an area in which icy crustal plates were separated, rotated, and moved into new positions (Schenk and Seyfort 1980, Pieri 1981, Schenk and McKinnon 1989, Golombek and Banerdt 1990, Pappalardo and Sullivan 1996) reminiscent of ice packs in the polar seas of Earth. This area was imaged by Galileo at 420 m/pixel and 1.6 km/pixel and includes dark bands as wide as 35 km. Sullivan *et al.* (1997) and Tufts *et al.* (1997) show that reconstruction of the plates into prefractured configurations can be accomplished with little or no overlap of plate margins. However, they also note that a small part of bright plains material is missing and apparently has been consumed or altered (i.e., darkened). The bilateral symmetry of some dark bands suggests patterns similar to those of sea-floor spreading, in which fractures repeatedly open

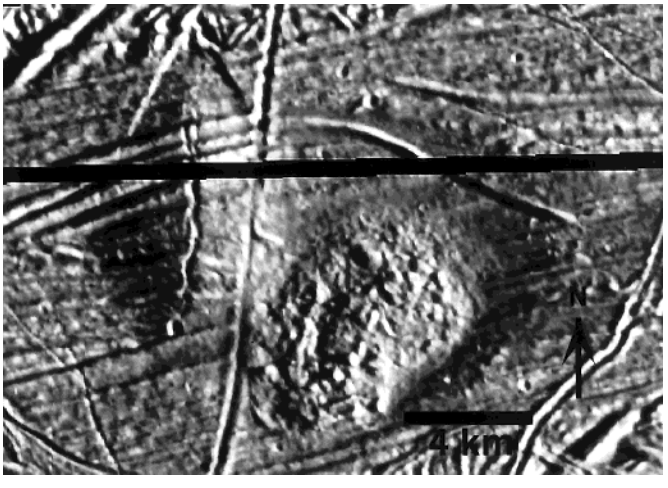

FIG. 13. Area centered at 9°N, 276°W showing two features similar to those in Figure 11, interpreted to represent stages of endogenic deformation of the surface (area shown is 20 by 14 km) (JPL P-48525).

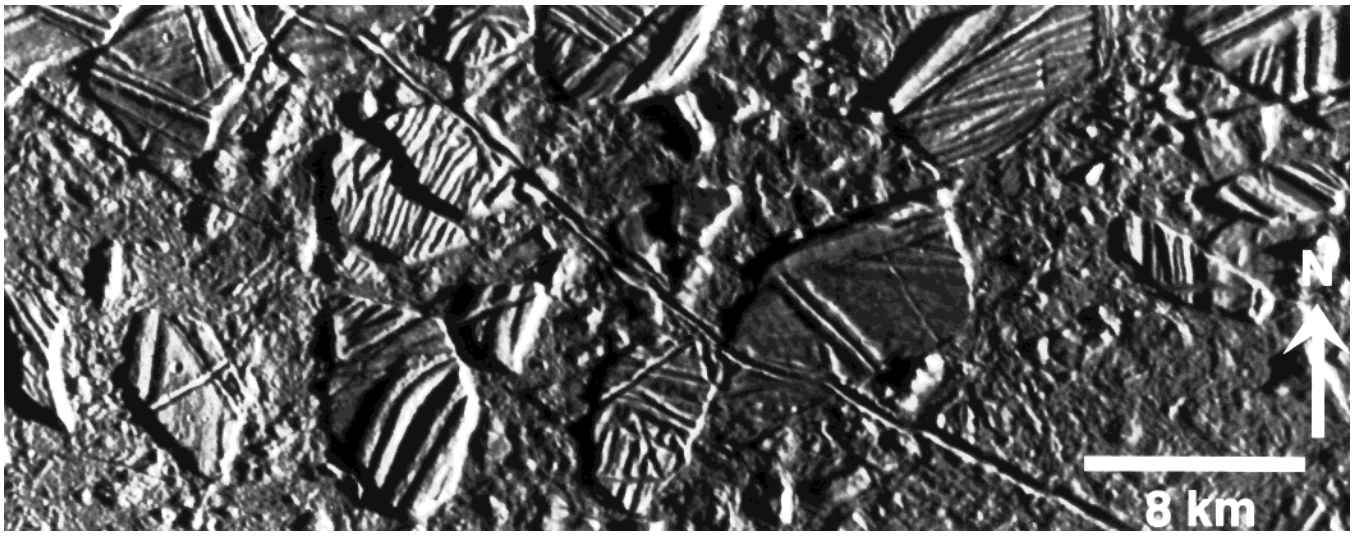

FIG. 14. High resolution (54 m/pixel) view of part of Conamara Chaos, the disrupted terrain seen in Figure 4 showing individual blocks of crust that have been broken apart and apparently ''rafted'' to new positions. The area shown in this picture is about 46 by 18 km; the small size of the blocks suggests that the depth to either liquid water or mobile ice was relatively shallow (a few km or less) at the time of disruption. Illumination from the right (from Belton *et al*. 1997; JPL P-48526).

along a spreading axis and are replaced with new material from the interior. The dark bands are thus gaps between laterally moving blocks rather than graben.

IMPACT CRATER DISTRIBUTIONS AND SURFACE AGES

Estimating ages of planetary surfaces is critical to the derivation of geologic history and understanding the evolution of planets and satellites. In the absence of planetary samples from which radiometric dates can be obtained, other, less direct techniques must be used to estimate ages of planetary surfaces. Crater size–frequency distributions are commonly used for this purpose (e.g., Hartmann *et al*. 1981). Calibrating the crater counts, however, is a problem, especially for the outer Solar System. Two approaches can be used, extrapolation from the Moon, where crater counts for surfaces have been calibrated using radiogenic dates from Apollo and Luna samples, and derivations based on current estimates of impact flux in the environment of interest—in this case, the jovian system. Both approaches must take into account various factors such as gravity scaling and potential satellite leading–trailing hemisphere asymmetries in impact flux and energies. Despite these and other uncertainties and assumptions, ages derived from crater counts enable comparisons among planetary surfaces if applied consistently, and they give insight into geological histories.

Crater size–frequency data were obtained for Callisto, Ganymede, and Europa (Neukum *et al*. 1998) for craters as small as 50 m in diameter using Galileo images and combined with previous measurements from Voyager images (Neukum 1983, 1985, Wagner *et al*. 1989). Size–frequency distributions of craters smaller than a few kilometers show a characteristic steep slope similar to those for the asteroids Gaspra and Ida (Chapman *et al*. 1996a, 1996b) and the inner Solar System planets, especially the Earth's moon (Neukum *et al*. 1975, Neukum 1983, Neukum

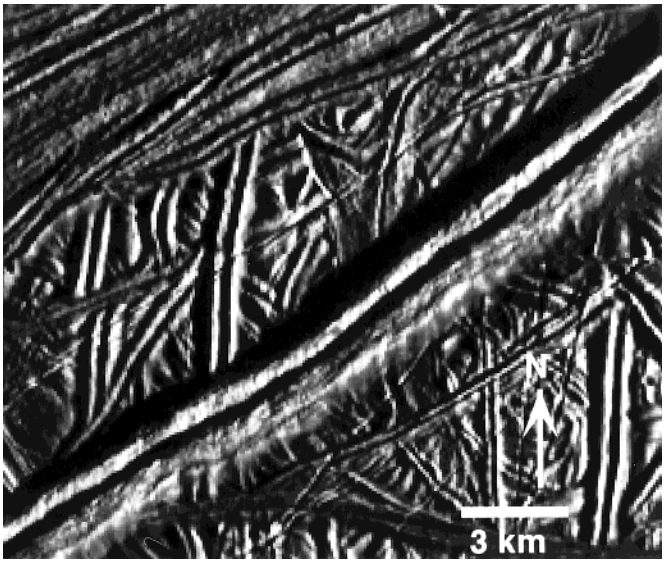

FIG. 15. High resolution (16 m/pixel) view of complex ridged terrain. The prominent ridge has a medial fracture and sets of smaller fractures paralleling both sides. Area shown is 18 by 15 km, illumination from the right of picture (Galileo image S038378652).

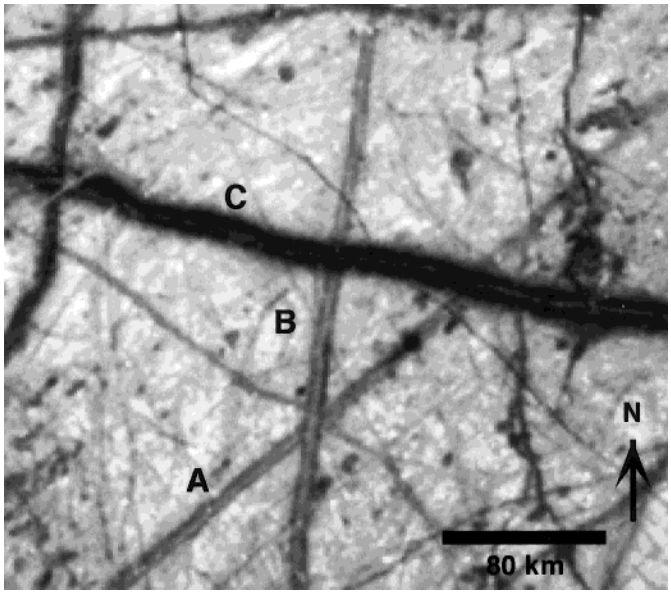

FIG. 16. Three intersecting triple bands; cross cutting relations show that the sequence of formation from oldest to youngest was A, B, C; note that with time, the low albedo component appears to brighten. Area shown is 320 by 280 km (Galileo image S0349875139).

and Ivanov 1994). Neukum et al. (1998) suggest that the distribution of impactors on the jovian moons is similar to that observed in the inner Solar System, including the asteroid belt. They note that the crater record on different geologic units of Ganymede and Callisto varies as much as an order of magnitude. In contrast, crater distributions on Europa are more uniform, with variations for three sites being less than a factor of four. Even on some of the youngest areas, impact craters can be identified, although the number of craters is 1/5 to 1/10 that of young maria of Earth's moon.

The crater counts for Europa can be used to estimate ages using the two approaches outlined above. In the one approach (extrapolation backward through time from present-day flux), applying Shoemaker's (1996) most recent value for the production of 10-km diameter craters to crater counts on Galileo images results in a surface age for Europa of about 10 million years. If the same rate is adjusted to Ganymede (~1.5 lower flux) and Callisto (~1.5 lower flux), then ages for young terrain on Ganymede are 230 myr to 2.3 byr, but the oldest dark terrain on Callisto is only about 3.2 byr old (Neukum 1997).

In the other approach, one can assume an age of 3.8 byr for the youngest large basin on Ganymede (Gilgamesh), which probably represents the last stage of heavy bombardment, equivalent approximately to the formation of the Orientale basin on the Moon. In addition, one can assume a lunar-like impact rate decay (Neukum 1983, Neukum and Ivanov 1994) with a half-life of about 100 myr between 4.5 and 3 byr ago and a constant flux for more recent times. These assumptions are based on a similar size–frequency distribution as in the inner Solar System and the same probable impactor source from the asteroid belt during the period of heavy bombardment. This is thought to dominate the cratering record if cometary cratering in the past 3 byr is relatively low. These assumptions lead to consistent results for all three Galilean satellites. The surface of Callisto then is 4.3 to 3.9 byr old (i.e., if the youngest basin-size impact occurred 3.9 byr ago); ages on Ganymede range from 4.2 byr for Galileo Regio to 3.7 byr for the youngest sulcus. Europa in this scenario is considerably younger than Ganymede and Callisto, but is still some 3.3 to 3 byr old.

Thus, unfortunately, the two approaches lead to very different ages for the europan surface—as young as 10^7 to as old as 3×10^9 years.

REGIONAL/GLOBAL TECTONIC PATTERNS

The lineae on Europa appear to be mostly ridges and fractures resulting from tectonic processes (Smith *et al.* 1979a, 1979b, Luchitta and Soderblom 1982, Pieri 1981). The formation of lineae has been variously ascribed to global expansion as a result of phase changes or dehydration of the interior (Finnerty *et al.* 1991), global contraction as a result of global cooling (Helfenstein and Parmentier 1983), polar wandering (Ojakangas and Stevenson 1989), and tidal stresses caused by Europa's orbital eccentricity (Helfenstein and Parmentier 1983, 1985, McEwen 1986b).

For a spherically symmetrical Europa in synchronous rotation, the pattern of fractures due to tidal stresses and orbital recession should be symmetrical about the antijovian longitude, and the jovian and antijovian hemispheres should have similar fracture patterns (Helfenstein and Parmentier 1983). Galileo images, however, do not show this distribution. If there is any symmetry on the better imaged antijovian hemisphere, it appears to be centered at about 205°W longitude. Moreover, the jovian and antijovian hemispheres appear fractured to different degrees, although this could be simply an effect of inadequate Voyager and Galileo image coverage and resolution. The offset of the longitude of symmetry from the antijovian longitude might be explained by nonsynchronous rotation. Because of the tides and the eccentric orbit, torques averaged over one orbit are nonzero (Yoder 1979, Greenberg and Wiedenschilling 1984). This could cause a slight difference in the orbital and rotational periods and slow nonsynchronous rotation (Geissler *et al.* 1998, Greenberg *et al.* 1998). The entire body could rotate nonsynchronously, or the ice crust could slowly rotate over a silicate interior that is in synchronous rotation. In both of these cases the stress fields caused by the tides and orbital recession will move slowly across the surface (Helfenstein and Parmentier

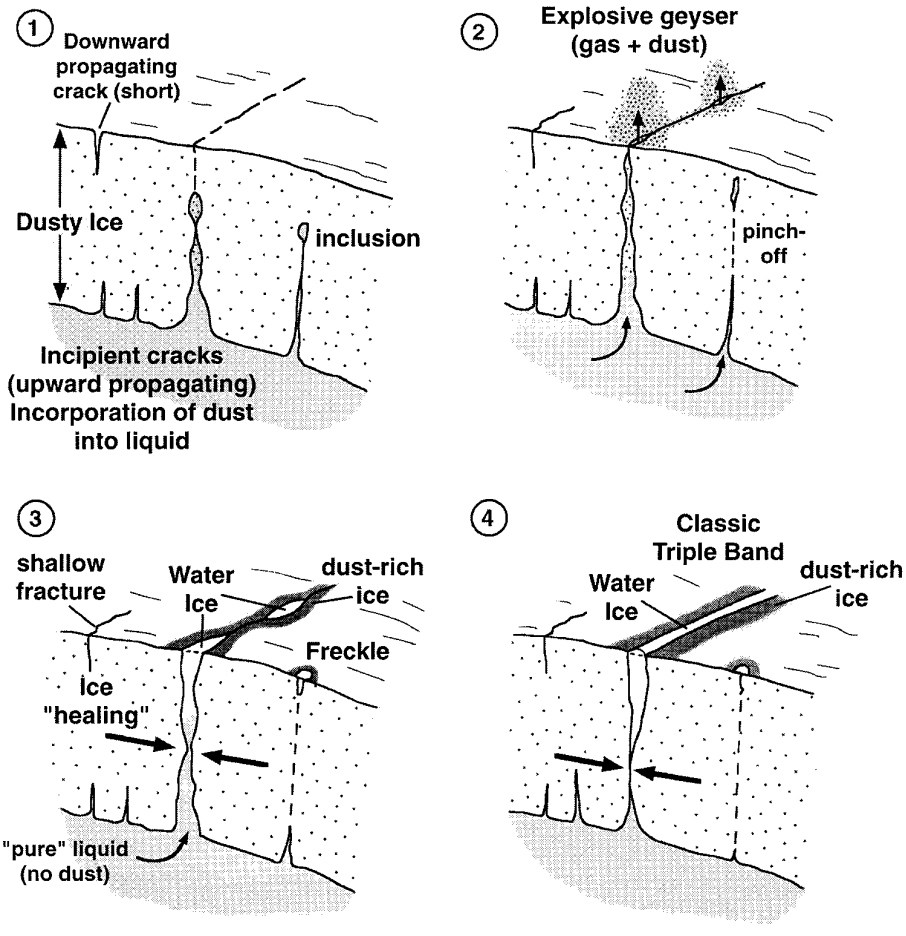

FIG. 17. Diagrams showing possible mode of formation for some triple bands.

1985) and, over time, all longitudes should experience the same stress pattern.

None of the proposed models (expansion, contraction, orbital recession coupled with synchronous or nonsynchronous rotation polar wandering), nor combinations thereof, fully explain the patterns of lineae observed in the Galileo images. Lack of symmetry about the jovian and antijovian points and lack of similarity between the jovian and antijovian hemispheres appear to rule out expansion and contraction coupled with synchronous rotation as the sole causes of the fracture pattern (Greenberg *et al.* 1997). A better fit is obtained if stress trajectories for nonsynchronous rotation are displaced eastward by 25°, as if the fractures preserved a record of nonsynchronous rotation from a previous epoch (McEwen 1986b), but this implies that the fractures formed by a mechanism that has ceased, which would be inconsistent with a young age of much of the surface.

Greenberg *et al.* (1998) and Geissler *et al.* (1998) mapped the stress fields that result from the combination of stresses accumulating from nonsynchronous rotation and ''diurnal'' stresses due to Europa's eccentric orbit. They found that the orientations of major lineament systems, as well as time sequences of crack formation inferred from Galileo images, fit a model in which cracking occurred at various times during the last 90° of rotation relative to the direction of Jupiter. The success of that model supports the possibility of on-going nonsynchronous rotation as well as the important role played by both nonsynchronous and diurnal tidal stress.

None of the proposed mechanisms explain fractures and boundaries between surface units that outline the circular structure at 20°S, 203°W, described earlier. One possibility is that the silicate subcrust that underlies the ice crust is not homogeneous and does not form a smooth surface, but instead retains a record of cratering from Europa's early history. Inhomogeneities in the silicate subcrust and the topography of the silicate surface might have influenced the way in which the icy crust responds to the tidal stresses. We suggest that the circular pattern could reflect an ancient impact basin in the silicate subcrust. Such a basin could be located close to the antijovian point because the basin

FIG. 18. View of a ''pull-apart'' zone near the anti-Jovian region showing parts of the europan surface that have been separated. The prominent dark wedge shows bilateral symmetry of its ridges and grooves, suggesting repeated separation and infilling; area shown is 238 by 225 km; illuminated from the west (left) (Galileo image S0368639400; JPL P-48127).

results in a center of mass offset, thereby locking at least the silicate interior in its present orientation with respect to Jupiter.

A subsurface impact scar could influence the deformation of the ice crust in at least two ways. If the crust is mechanically coupled to the silicate subcrust, then tidal stresses in both the crust and subcrust would tend to be relieved along previously formed dislocations, and dislocations in the silicate subcrust would propagate upward into the ice. On the other hand, if the ice crust is decoupled from the silicate interior by a melt zone or ''ocean'' (Squyres *et al*. 1993), then the tidal stresses would be relieved mostly within the ice crust and ancient fractures could not propagate upward into the ice. However, topography on the silicate subcrust could influence the way that the ice crust deformed so that the fracture pattern is the result of current, or recent, tidal stresses as modified by flexure of the crust and interaction of the low viscosity ''ocean'' layer with the topography of an ancient multiringed basin in the silicate subcrust.

Summary

How then can the questions about Europa posed in the Introduction be addressed?

Information on the interior comes primarily from geo-

physical measurements. The close flybys of the Galileo spacecraft provide some measurements, including moments of inertia (Anderson *et al.* 1997), which suggest that the interior is differentiated into a large core about half the radius of the satellite, a small rocky mantle, and an outer H_2O-rich shell. These results are consistent with the variety and morphology of the surface features revealed in images, including ridges and fractures resulting from tectonic processes, and cryovolcanic features including possible flows. Ejecta patterns from fresh impact craters suggest lateral and vertical heterogeneity in mixtures of ice and nonice materials in the upper ($<$15 km) H_2O shell of Europa.

It is not known if liquid water exists below the surface today. However, the presence of lobate and possible extrusive features indicates that temperatures were sufficiently high to melt or ''soften'' ice at or close to the surface in geologically recent times. These features do not occur everywhere on the surface, and liquid or warm zones could be local rather than global.

The geological evolution of Europa is complex. The icy lithosphere has been tectonically modified by fracturing and faulting, including lateral displacement along shear zones (Tufts 1996) and disruption in local spreading centers especially in the antijovian hemisphere. Various linear features such as ridges are seen at all scales from global (thousands of kilometers long) to local at the limits of resolution (tens of meters). Remnants of ridged and grooved terrain attest to tectonic deformation throughout the history of the satellite. Differences in crater size–frequency distributions suggest that some areas have been more active than others. However, until global geologic mapping is achieved, knowledge of the evolution of the Europan surface remains rudimentary.

There has been considerable speculation regarding the possibility of current cryovolcanic activity on Europa. Most ideas derive from models of interior heating (e.g., Cassen *et al.* 1982, Schubert *et al.* 1986). Thus far, the Galileo data leave the matter unresolved. However, the strategy developed for the imaging experiment through the Galileo Europa Mission (GEM) includes searching for potential changes on the surface and targeting areas that might be sites of cryovolcanic activity. We are also imaging Europa while it is in Jupiter's shadow to search for current activity that might be detected by light scattered from erupting particles. Unfortunately, the amount of data is very limited and an extensive campaign to search for activity is not possible.

The Galileo Europa Mission will pave the way for future exploration. After the nominal mission ended in 1997, current plans call for continued operation of the Galileo spacecraft with multiple flybys of Europa and ending with close encounters with Io. The multiple Europa flybys will increase the observations of its surface both in space and time to evaluate the likelihood of current activity and refine geophysical measurements to increase knowledge of the interior. High-resolution images in stereoscopic views and in color will enable the targeting of scientifically interesting regions for future exploration, ultimately perhaps including landed operations.

ACKNOWLEDGMENTS

We thank the dedicated members of the Galileo project who enabled the acquisition of images for Europa. In particular, we are grateful to Herb Brenneman, David Senske, Jim Kaufman, Todd Jones, and Kari Magee for tireless work in implementing the complex sequences in order to extract the maximum quality data from the limited available resources. We appreciate the review of the manuscript and the insight provided by Jeff Kargel. We thank Byrnece Erwin, Keith Rust, and Andrea Gorman for word processing and associates of imaging team members who contributed to the illustrations, including Cynthia Phillips, Kim Homan, Sue Selkirk, Helen Mortenson, and Amy Culver.

REFERENCES

Anderson, J. D., E. L. Lau, W. L. Sjorgren, G. Schubert, and W. B. Moore 1997. Europa's differentiated internal structure: Inferences from two Galileo encounters. *Science* **276,** 1236–1239.

Belton, M. J. S., and 22 colleagues 1992. The Galileo solid-state imaging experiment. *Space Sci. Rev.* **60,** 413–455.

Belton, M. J. S., and the SSI Team 1996. Galileo's first images of Jupiter and the Galilean satellites. *Science* **274,** 377–385.

Buratti, B., and M. Golombek 1988. Geologic implications of spectrophotometric measurements on Europa. *Icarus* **75,** 437–449.

Carr, M. H., and the SSI Team 1995. The Galileo Imaging team plan for observing the satellites of Jupiter. *J. Geophys. Res.* **100,** 18,935–18,955.

Carr, M. H., F. Chuang, M. Belton, K. Bender, C. Chapman, R. Greeley, A. McEwen, R. Sullivan, and the Galileo Imaging Team 1997. A large multi-ringed structure on Europa: A possible remnant of an impact basin buried beneath the ice crust. *Lunar Planet. Sci. Conf.* XXVIII, pp. 207–208. [Abstract]

Carr, M. H., M. J. S. Belton, C. R. Chapman, M. E. Davies, P. Geissler, R. Greenberg, A. S. McEwen, B. R. Tufts, R. Greeley, R. Sullivan, J. W. Head, R. T. Pappalardo, K. P. Klaasen, T. V. Johnson, J. Kaufmann, D. Senske, J. Moore, G. Neukum, G. Schubert, J. A. Burns, P. Thomas, and J. Veverka 1998. New evidence for a global ocean on Europa. *Nature* **391,** 363–365.

Cassen, P. M., R. T. Reynolds, and S. J. Peale 1979. Is there liquid water on Europa? *Geophys. Res. Lett.* **6,** 731–734.

Cassen, P. M., S. J. Peale, and R. T. Reynolds 1982. Structure and thermal evolution of the Galilean satellites. In *Satellites of Jupiter* (D. Morrison, Ed.), pp. 93–128. Univ. of Arizona Press, Tucson.

Chapman, C. R., J. Veverka, M. J. S. Belton, G. Neukum, and D. Morrison 1996a. Cratering on Gaspra. *Icarus* **120,** 231–245.

Chapman, C. R., E. V. Ryan, W. J. Merline, G. Neukum, R. Wagner, P. C. Thomas, J. Veverka, and R. J. Sullivan 1996b. Cratering on Ida. *Icarus* **120,** 77–86.

Chapman, C. R., W. J. Merline, B. Bierhaus, J. Keller, S. Brooks, A. McEwen, B. R. Tufts, J. Moore, M. Carr, R. Greeley, K. C. Bender, R. Sullivan, J. Head, R. Pappalardo, M. J. S. Belton, G. Neukum, R. Wagner, C. Pilcher, and the Galileo Imaging Team 1997. Populations of small craters on Europa, Ganymede, and Callisto: Initial Galileo

imaging results. *Lunar Planet. Sci. Conf.* XXVIII, pp. 217–218. [Abstract]

Clark, B. E., P. Helfenstein, J. Veverka, P. Geissler, M. Bell, R. Greeley, R. Sullivan, T. Denk, A. S. McEwen, C. B. Phillips, and the Galileo Imaging Team 1997. Multispectral behavior and mixing model simulations of Europan terrains from Galileo images. *Lunar Planet. Sci. Conf.* XXVIII, pp. 235–236. [Abstract]

Crawford, G. D., and D. J. Stevenson 1988. Gas-driven water volcanism and the resurfacing of Europa. *Icarus* **73,** 66–79.

Croft, S. K. 1983. A proposed origin for palimpsests and anomalous pit craters on Ganymede and Callisto. *Lunar Planet. Sci. Conf.* XIV, *J. Geophys. Res. Suppl.* **88,** B17–B89.

Davies, M. E. 1982. Cartography and nomenclature for the Galilean satellites. In *Satellites of Jupiter* (D. Morrison, Ed.), pp. 911–933. Univ. of Arizona Press, Tucson.

Fanale, F. P., and 22 colleagues 1998. Galileo's multi-instrument spectral view of Europa's surface composition. *Icarus*, submitted.

Fink, U., N. H. Dekkers, and H. P. Larson 1973. Infrared spectra of the Galilean satellites of Jupiter. *Astrophys. J.* **179,** L154–L155.

Finnerty, A. A., G. A. Ransford, D. C. Pieri, and K. D. Collerson 1981. Is Europa surface cracking due to thermal evolution? *Nature* **289,** 24–27.

Geissler, P. E., M. Bell, M. J. S. Belton, J. Burns, B. Clark, T. Denk, R. Greeley, R. Greenberg, P. Helfenstein, A. McEwen, R. Pappalardo, R. Sullivan, R. Tufts, J. Veverka, and the Galileo Imaging Team 1997. Galileo multispectral imaging of Europa: Evidence for non-synchronous rotation. *Lunar Planet. Sci. Conf.* XXVIII, pp. 401–402. [Abstract]

Geissler, P. E., R. Greenberg, G. Hoppa, P. Helfenstein, A. McEwen, R. Pappalardo, R. Tufts, M. Bell, R. Sullivan, R. Greeley, M. J. S. Belton, T. Denk, B. Clark, J. Burns, J. Veverka, and the Galileo Imaging Team 1998. Evidence for non-synchronous rotation of Europa: Indications from Galileo observations. *Nature* **391,** 368–369.

Golombek, M. P., and W. B. Banerdt 1990. Constraints on the subsurface structure of Europa. *Icarus 8***3,** 441–452.

Golombek, M. P., and E. Bruckenthal 1983. Origin of triple bands on Europa. *Lunar Planet. Sci. Conf.* XIV, pp. 251–252. [Abstract]

Greeley, R., and the Galileo SSI Team 1996. Europa: First Galileo views. Europa Ocean Conference, pp. 32–33, San Juan Capistrano Res. Inst.

Greeley, R., J. H. Fink, D. E. Gault, and J. E. Guest 1982. Experimental simulation of impact cratering on icy satellites. In *Satellites of Jupiter* (D. Morrison, Ed.), pp. 340–378. Univ. of Arizona Press, Tucson.

Greenberg, R., and S. J. Wiedenschilling 1984. How fast do Galilean satellites spin? *Icarus* **58,** 186–196.

Greenberg, R., P. Geissler, R. Pappalardo, and the Galileo Imaging Team 1997. Long term and ''diurnal'' tidal stresses on Europa. *Lunar Planet. Sci. Conf.* XXVIII, pp. 457–458. [Abstract]

Greenberg, R., P. Geissler, G. Hoppa, B. R. Tufts, D. D. Durda, R. Pappalardo, J. W. Head, R. Greeley, R. Sullivan, and M. Carr 1998. Tectonic processes on Europa: Tidal stresses, mechanical response, and visible features. *Icarus* **135,** 64–78.

Hartmann, W. K., R. G. Strom, S. J. Weidenschilling, K. R. Blasius, A. Woronoco, M. R. Dence, R. A. F. Grieve, J. Diaz, C. R. Chapman, E. M. Shoemaker, and K. L. Jones 1981. Chronology of planetary volcanism by comparative studies of planetary cratering. In *Basaltic Volcanism on the Terrestrial Planets*, pp. 1048–1127. Pergamon, New York.

Helfenstein, P., and E. M. Parmentier 1980. Fractures on Europa: Possible response of an ice crust to tidal deformation. *Proc. Lunar Planet. Sci. Conf. 11th*, pp. 1987–1998.

Helfenstein, P., and E. M. Parmentier 1983. Patterns of fracture and tidal stresses on Europa. *Icarus* **53,** 415–430.

Helfenstein, P., and E. M. Parmentier 1985. Patterns of fracture and tidal stresses due to nonsynchronous rotation: Implications for fracturing on Europa. *Icarus* **61,** 175–184.

Jones, K. B., J. W. Head, C. R. Chapman, R. Greeley, J. M. Moore, G. Neukum, R. T. Pappalardo, and the Galileo SSI Team 1997. Morphology of palimpsests on Ganymede from Galileo observations. *Lunar Planet. Sci. Conf.* XXVIII, pp. 679–680. [Abstract]

Kargel, J. S. 1991. Brine volcanism and the interior structures of asteroids and icy satellites. *Icarus* **94,** 368–390.

Kargel, J. S. 1995. Cryovolcanism on the icy satellites. *Earth Moon Planets* **67,** 101–113.

Kargel, J. S., S. K. Croft, J. I. Lunine, and J. S. Lewis 1991. Rheological properties of ammonia-water liquids and crystal-liquid slurries: Planetological applications. *Icarus* **89,** 93–112.

Klaasen, K. P., M. C. Clary, and J. R. Janesick 1984. Charge-coupled device television camera for NASA's Galileo mission to Jupiter. *Opt. Eng.* **23,** 334–342.

Klemaszewski, J. E., R. Greeley, and the SSI Team 1997. Topography of europan brown and gray mottled terrains from Galileo images at low sun illumination. *Lunar Planet. Sci. Conf.* XXVIII, pp. 739–740. [Abstract]

Lanzerotti, L. J., W. L. Brown, J. M. Poate, and W. M. Augustyniak 1978. On the contribution of water products from Galilean satellites to the jovian magnetosphere. *Geophys. Res. Lett.* **5,** 155–158.

Leith, A. C., and W. B. McKinnon 1996. Is there evidence for polar wander on Europa? *Icarus* **120,** 387–398.

Lucchitta, B. K., and L. A. Soderblom 1982. Geology of Europa. In *Satellites of Jupiter* (D. Morrison, Ed.), pp. 521–555. Univ. of Arizona Press, Tucson.

Lucchitta, B. K., L. A. Soderblom, and H. M. Ferguson 1981. Structures on Europa. *Proc. Lunar Planet. Sci. 12B,* pp. 1555–1567.

Malin, M. C., and D. C. Pieri 1986. Europa. In *Satellites* (J. A. Burns and M. S. Matthews, Eds.), pp. 689–716. Univ. of Arizona Press, Tucson.

McCord, T. B., G. B. Hansen, F. P. Fanale, R. W. Carlson, D. L. Matson, T. V. Johnson, W. D. Smythe, J. K. Crowley, P. D. Martin, A. Ocampo, C. A. Hibbitts, J. C. Granahan, and the NIMS Team 1998. Salts on Europa's surface detected by Galileo's near infrared mapping spectrometer. *Science* **280,** 1242–1245.

McEwen, A. S. 1986a. Exogenic and endogenic albedo and color patterns on Europa. *J. Geophys. Res.* **91,** 8077–8097.

McEwen, A. S. 1986b. Tidal reorientation and the fracturing of Jupiter's moon Europa. *Nature* **321,** 49–51.

Melosh, H. J. 1989. *Impact Cratering.* Oxford University Press, Oxford.

Melosh, H. J., and W. B. McKinnon 1978. The mechanics of ringed basin formation. *Geophys. Res. Lett.* **5,** 985–988.

Moore, J. M., K. C. Bender, R. J. Sullivan, R. Greeley, A. S. McEwen, B. R. Tufts, J. W. Head III, R. T. Pappalardo, M. J. S. Belton, and the Galileo SSI Team 1997. Europan macula: Possible origins. *Lunar Planet. Sci. Conf.* XXVIII, pp. 973–974. [Abstract]

Murray, J. B. 1975. Near observations of surface markings on Jupiter's satellites. *Icarus* **25,** 397–404.

Neukum, G. 1983. *Meteoritenbombardment und Datierung planetarer Oberflaechen.* Habilitation Dissertation for Faculty Membership, Ludwig-Maximilians-University of Munich, Germany.

Neukum, G. 1985. Cratering records of the satellites of Jupiter and Saturn. *Adv. Space Res.* **5,** 107–116.

Neukum, G. 1997. Bombardment history of the jovian system. In *The Three Galileos: The Man, the Spacecraft, the Telescope* (C. Barbieri, J. H. Rahe, T. V. Johnson, and A. M. Sohus, Eds.), pp. 201–212. Kluwer Academic, Dordrecht.

Neukum, G., and B. A. Ivanov 1994. Crater size distributions and impact probabilities on Earth from lunar, terrestrial-planet, and asteroid cratering data. In *Hazards Due to Comets and Asteroids* (T. Gehrels, Ed.), pp. 359–416. Univ. of Arizona Press, Tucson.

Neukum, G., B. Koenig, and J. Arkani-Hamed 1975. A study of lunar impact crater size-distributions. *The Moon* **12,** 201–229.

Neukum, G., R. Wagner, U. Wolf, J. W. Head, R. Pappalardo, C. R. Chapman, W. J. Merline, R. Greeley, M. J. S. Belton, and the Galileo SSI Team 1998. Bombardment history and ages of the Galilean satellites. *Ann. Geophys.* **16,** Suppl. III, C-993. [Abstract]

Ojakangas, G. W., and D. J. Stevenson 1989. Thermal state of an ice shell on Europa. *Icarus* **81,** 220–241.

Pappalardo, R., and M. D. Coon 1996. A sea ice analog for the surface of Europa. *Lunar Planet. Sci. Conf.* XXVII, pp. 997–998. [Abstract]

Pappalardo, R., and R. Sullivan 1996. Evidence for separation across a gray band on Europa. *Icarus* **123,** 557–567.

Pappalardo, R. T., J. W. Head, R. Greeley, R. J. Sullivan, C. Pilcher, G. Schubert, W. Moore, M. H. Carr, J. M. Moore, M. J. S. Belton, and D. L. Goldsby 1998. Geological evidence for solid-state convection in Europa's ice shell. *Nature* **391,** 365–368.

Passey, Q. R., and E. M. Shoemaker 1982. Craters and basins on Ganymede and Callisto: Morphological indicators of crustal evolution. In *Satellites of Jupiter* (D. Morrison, Ed.), pp. 379–434. Univ. of Arizona Press, Tucson.

Pieri, D. C. 1981. Lineament and polygon patterns on Europa. *Nature* **289,** 17–21.

Pilcher, C. B., S. T. Ridgway, and T. B. McCord 1972. Galilean satellites: Identification of water frost. *Science* **178,** 1087–1089.

Schenk, P. M., and W. B. McKinnon 1989. Fault offsets and lateral crustal movement on Europa: Evidence for a mobile ice shell. *Icarus* **79,** 75–100.

Schenk, P. M., and C. K. Seyfert 1980. Fault offsets and proposed plate motions for Europa. *EOS Trans. Amer. Geophys. Union* **61,** 286.

Schubert, G., T. Spohn, and R. T. Reynolds 1986. Thermal histories, compositions, and internal structures of the moons of the Solar System. In *Satellites* (J. A. Burns and M. S. Matthews, Eds.), pp. 224–292. Univ. of Arizona Press, Tucson.

Shoemaker, E. M. 1996. The age of Europa's surface. Europa Ocean Conf., San Juan Capistrano, Nov. 12–14, pp. 65–66.

Shoemaker, E. M., and R. F. Wolfe 1982. Cratering time scales for the Galilean satellites. In *Satellites of Jupiter* (D. Morrison, Ed.), pp. 277–339. Univ. of Arizona Press, Tucson.

Simonelli, D. P., J. Veverka, D. A. Senske, F. P. Fanale, G. Schubert, and M. J. S. Belton 1998. Galileo search for SO_2-frost condensation on Io's nightside. *Icarus* **135,** 166–174.

Smith, B. A., L. A. Soderblom, T. V. Johnson, A. Ingersoll, S. A. Collins, E. M. Shoemaker, G. E. Hunt, H. Masursky, M. Carr, M. E. Davies, A. F. Cook, J. Boyce, G. E. Danielson, T. Owen, C. Sagan, R. Beebe, J. Veverka, R. Strom, J. McCauley, D. Morrison, G. Briggs, and V. E. Soumi 1979a. The Jupiter system through the eyes of Voyager 1. *Science* **204,** 951–972.

Smith, B. A., L. A. Soderblom, R. Beebe, J. Boyce, G. Briggs, M. Carr, S. A. Collins, A. F. Cook, G. E. Danielson, M. E. Davies, G. E. Hunt, A. Ingersoll, T. V. Johnson, H. Masursky, J. McCauley, D. Morrison, T. Owen, C. Sagan, E. M. Shoemaker, R. Strom, V. E. Soumi, and J. Veverka 1979b. The Galilean satellites and Jupiter: Voyager 2 imaging results. *Science* **206,** 927–950.

Spencer, J. R., W. M. Calvin, and M. J. Person 1995. Charge-coupled device spectra of the Galilean satellites: Molecular oxygen on Ganymede. *J. Geophys. Res.* **100,** 19,049–19,056.

Squyres, S. W. 1980. Surface temperatures and retention of H_2O frost on Ganymede and Callisto. The satellites of Jupiter. *IAU Coll.* **57.**

Squyres, S. W., R. T. Reynolds, P. Cassen, and S. J. Peale 1983. Liquid water and active resurfacing on Europa. N*ature* **301,** 225–226.

Stofan, E. R., V. L. Sharpton, G. Schubert, G. Baer, D. L. Bindschadler, D. M. Janes, and S. W. Squyres 1992. Global distribution and characteristics of coronae and related features on Venus: Implications for origin and relation to mantle processes. *J. Geophys. Res.* **97,** 13,347–13,378.

Sullivan, R., M. Belton, K. Bender, M. Carr, C. Chapman, R. Greeley, J. Head, K. Homan, J. Moore, R. Pappalardo, B. R. Tufts, and the GLL SSI Team 1997. Galileo views of crustal disruption on Europa. *Lunar Planet. Sci. Conf.* XXVIII, pp. 1395–1396. [Abstract]

Tufts, B. R. 1996. A San-Andreas-sized strike-slip fault on Europa. *Lunar Planet. Sci. Conf.* XXVII, pp. 1343–1344. [Abstarct]

Tufts, B. R., R. Greenberg, R. Sullivan, R. Pappalardo, and the Galileo Imaging Team 1997. Reconstruction of Europan terrain in the Galileo C3 "wedges" image and its geological implications. *Lunar Planet. Sci. Conf.* XXVIII, pp. 1455–1456. [Abstract]

Wagner, R., K. Schmidt, and G. Neukum 1989. Crater retention ages of geologic units on Ganymede and Callisto. *AIAA/JPL 2nd Internat. Conf. on Solar System Expl. Abstracts*, California Inst. of Tech., Pasadena.

Wilson, L., J. W. Head, and R. T. Pappalardo 1997. Eruption of lava flows on Europa: Theory and application to Thrace Macula. *J. Geophys. Res.* **102,** 9263–9272.

Yoder, C. F. 1979. How tidal heating in Io drives the Galilean orbital resonance locks. *Nature* **279,** 767–770.

Zel'dovich, Ya.B., and Yu.P. Raizer 1967. *The Physics of Shock Waves and High-Temperature Hydrodynamic Phenomena*, Vol. II. Academic Press, New York.